**IL-13 promotes sensory-sympathetic neurons crosstalk in asthma**

Théo Crosson [1,2], Shreyas Bhat [2,3], Jo-Chiao Wang [1,2], Clara Salaun [1,2], Katiane Roversi [1,2], Herbert Herzog [4], Moutih Rafei [1], Rikard Blunck [2,3], Sebastien Talbot [1,2,5,6,#]

[1] Département de Pharmacologie et Physiologie, Université de Montréal, Canada.
[2] Centre Interdisciplinaire sur le Cerveau et l'Apprentissage (CIRCA), Université de Montréal, Canada.
[3] Département de Physique, Université de Montréal, Canada
[4] Gavan Institute of Medical Research, Australia.
[5] Department of Pharmacology and Physiology, Karolinska Institutet. Sweden.
[6] Department of Biomedical and Molecular Sciences, Queen's University. Canada.

[#] Lead Contact:
Sebastien Talbot, PhD
Phone: 438-521-3466
Email: sebas.talbot@gmail.com; sebastien.talbot@queensu.ca
ORCID: 0000-0001-9932-7174

**KEYWORDS.** Allergy, asthma, IL-6, IL-13, neuro-immunology, nociceptor neurons, NPY1R, vagus nerve.

**SHORT TITLE:** Cytokines reprogram nociceptor transcriptome

**CONFLICT OF INTEREST:** The authors have no conflict of interest.

**ABSTRACT.** Nociceptor neurons play a crucial role in maintaining the body's equilibrium by detecting and responding to potential dangers in the environment. However, this function can be detrimental during allergic reactions, since vagal nociceptors can contribute to immune cell infiltration, bronchial hypersensitivity, and mucus imbalance, in addition to causing pain and coughing. Despite this, the specific mechanisms by which nociceptors acquire pro-inflammatory characteristics during allergic reactions are not yet fully understood. In this study, we aimed to investigate the molecular profile of airway nociceptor neurons during allergic airway inflammation and identify the signals driving such reprogramming. Using retrograde tracing and lineage reporting, we identified a class of inflammatory vagal nociceptor neurons that exclusively innervate the airways. Using an ovalbumin mouse model of airway inflammation, we found that these neurons undergo significant reprogramming characterized by the upregulation of the NPY receptor *Npy1r*, along with *Il6*. A screening of asthma-driving cytokines revealed that IL-13 drives part of this reprogramming, including *Npy1r* overexpression via the JAK/STAT6 pathway, while IL-1β induces IL-6 expression and release. Additionally, we observed that sympathetic neurons release NPY in the bronchoalveolar fluid of asthmatic mice, which limits the excitability of nociceptor neurons. In summary, allergic airway inflammation reprograms airway nociceptor neurons to acquire a pro-inflammatory phenotype, characterized by the release of IL-6, while a compensatory mechanism involving NPY1R limits nociceptor neurons' activity.

**BACKGROUND.** Sensory neurons are heterogenous and can be differentiated based on their expression profiles (1-3), degree of myelination (4), the type of cues to which they are sensitive (4, 5), the reflexes that they initiate, their anatomical location (6) or the organ that they innervate (7, 8). For instance, internal organs such as the lungs are innervated by the vagus nerve, whose neurons originate from the jugular nodose complex ganglia (JNC).

Pain sensory neurons, also known as nociceptor neurons, form a key line of defense against environmental dangers. They detect a broad range of thermal, mechanical, and chemical threats and respond by means of protective reflexes such as the itch and cough reflexes (9, 10). To fulfill their role in host defense, nociceptors are geared to detect and respond to a variety of danger signals ranging from cytokines to inflammatory lipids, allergens, fungi, cancer cells, bacteria, toxins, and even immunoglobulins (5, 11, 12). Via the axon reflex, nociceptors respond by locally releasing neuropeptides. While these peptides can have direct inflammatory and immunomodulatory actions (13-19), nociceptors' impact on inflammation is also indirect, via modulation of the autonomic nervous system (20).

In the context of asthma, vagal nociceptors neurons worsen airway hyperreactivity by promoting bronchoconstriction, coughing, mucus imbalance, and immune cell infiltration(14, 21-23). Yet, the specific mechanisms by which nociceptors are activated and acquire this pro-inflammatory phenotype are not fully

understood. Here we sought to define the molecular profile of airway nociceptor neurons during allergic airway inflammation and to identify the signals driving their reprogramming.

Using retrograde tracing and lineage reporting, we first identified the population of nociceptor neurons that innervates the airways. Using the ovalbumin mouse model of allergic airway inflammation, we found drastic airway nociceptor neurons reprogramming characterized by the upregulation of the NPY receptor *Npy1r,* and the cytokine *Il6.* Next, we identified that the asthma-driving cytokine IL-13, via pSTAT6 signaling, drives part of this transcriptional reprogramming. Along with *Npy1r* overexpression, we found that NPY was elevated in the bronchoalveolar fluid of asthmatic mice. In cultured JNC neurons, NPY decreased nociceptor neurons cAMP and blunted neuronal excitability.

**RESULTS.** Via vagal projections, the JNC innervates most visceral organs (24). Single-cell RNA sequencing datasets revealed that JNC neurons are highly heterogenous (2, 3, 25) and provide a transcriptome-based neuron subtype classification (2, 3, 6, 26). While genetically guided optogenetic studies identified JNC neuronal subtypes controlling breathing and tracheal reflexes (1, 25), additional molecular characterization of airway nociceptors is lacking.

To address this, we tracked airway nociceptors using the $Na_V1.8^{cre}$::$tdTomato^{fl/wt}$ nociceptor neuron reporter mice, in which, we back-labeled airway neurons using the retrograde tracer DiD' (i.n. 200 µM). Two weeks after DiD' injection, the JNC neurons were isolated, and airway nociceptor neurons ($Na_V1.8^+DiD^+$), visceral nociceptor neurons ($Na_V1.8^+DiD^-$) and glial cells ($Na_V1.8^-$ , a mixed population including satellite glial cells, macrophages, stromal cells and $Nav1.8^{neg}$ neurons), were purified by flow cytometry (**SF. 1A-B**) and RNA-sequenced (**Fig. 1A-B, SF. 1C**). About 5–10% of JNC nociceptors neurons were labeled with DiD' (**SF. 1B, D**). PCA analysis confirmed that the three cell populations were well segregated (**SF. 1C**). When compared with visceral nociceptor neurons, *Il6, Kcng1*, *Trpa1, Trpv1,* and *Npy1r* were found to be significantly enriched in airway nociceptor neurons (**Fig. 1A-B**). Calcium imaging of JNC neurons showed that while capsaicin sensitivity was similar across neuronal subpopulations, JT010-mediated TRPA1 activation was drastically increased (2.5-fold) in airway neurons ($DiD^+$) compared to other visceral neurons (**Fig. 1C, SF. 1E-F**). Using JNC neurons from $NPY1R^{Cre}$::$tdTomato^{fl/wt}$ mice, we also confirmed NPY1R enrichment in the airway population (**Fig. 1D**).

We then mapped out the airway nociceptor neuron subsets within the JNC neuron populations using published scRNAseq data from Prescott and colleagues (1). We reanalyzed the data using *Vglut2, Scn10a* and *Scn1a* to define clusters of nociceptors and low-threshold sensory neurons (2), and *Phox2b* and *Prdm12* to differentiate between jugular and nodose neurons (**Fig. 1E**, **SF. 2A-D**) We found that the marker genes of one cluster, Nodose Nociceptor 8 (NN8), were highly enriched (Normalized Enrichment Score (NES)=2.2) in our airway nociceptor neurons sequencing (**Fig. 1E**). NN8 thus appears to exclusively innervate the airways. Several of NN8 markers (*Trpv1, Trpa1*; **Fig. 1E**) are known drivers of neurogenic inflammation in the airways (23, 27-30), while this cluster also co-expresses *Npy1r* and *Il6* (**Fig. 1E, SF. 2E-J**). Additionally, we identified three other populations of sensory neurons preferentially innervating the airways (**Fig. 1E)**, including a subset that we assume to be cough-inducing mechanoreceptors (NN7; **Supplementary table 1**).

Next, we sought to test whether the airway nociceptor neuron transcriptome is impacted during allergic airway inflammation (AAI). Retrograde tracer-exposed nociceptor reporter mice ($Na_V1.8^{cre}$::$tdTomato^{fl/wt}$) underwent the classic ovalbumin (OVA) model of asthma (14). OVA-exposed mice showed significant airway inflammation characterized by eosinophilic infiltration (**Fig. 2A**), but a similar number of back-labeled airway nociceptor neurons (**SF. 3A**). As previously defined (**SF. 1A-B**), the JNC neurons were isolated, and airway nociceptor neurons ($Na_V1.8^+DiD^+$), visceral nociceptor neurons ($Na_V1.8^+DiD^-$) and glial cells ($Na_V1.8^-$) were purified by flow cytometry and RNA-sequenced.

DESeq2 analysis revealed that AAI significantly affected the expression of 92 genes in airway nociceptor neurons (**Fig. 2B-E**), compared with only one and two genes in the visceral nociceptor neurons and glial cells population, respectively (**Fig. 2B, SF3. B-C**). Seventeen of these upregulated genes had previously been associated with increased pain or nociceptors activity, while six were observed to dampen pain sensation (**Supplementary table 2**). Within the airway nociceptor neurons, AAI increased the expression of *Bdnf, Il6, Kcng1*, *Npy1r*, *Sting1,* and *Trpa1* (**Fig. 2C-D**). Notably, we also observed the enrichment of a nerve injury signature (31) (NES=2.0) including *Adcyap1*, *Adam8* or *Sox11* (**SF. 3D-E, Supplementary Table 3**).

Since the transcriptome changes induced by AAI are restricted to airway nociceptors and are virtually absent in other visceral nociceptors and glial cells, these variations are likely triggered by a mediator in the airways detected by peripheral nerve endings. To identify this neuromodulator, we exposed (24h) cultured JNC neurons to various allergy driving cytokines, inflammatory lipids, and neurotrophins, and used transcription changes to *Npy1r*, *Sting1*, *Bdnf*, and *Il6* as proxies for an AAI-like signature (**Fig. 2C**). IL-4 and IL-13 share the same receptor (IL4RII) and were found to increase *Npy1r* expression (**Fig. 3A**). We confirmed this observation by exposing cultures of JNC nociceptor neurons ($Na_V1.8^{cre}$::$tdTomato^{fl/wt}$) to IL-13. When compared with vehicle-exposed nociceptor neurons ($tdTomato^+$), IL-13 (24h) significantly affected the expression of 47 genes, including *Npy1r* (**Fig. 3B-C, Supplementary table 4**). Gene set enrichment analysis (GSEA) confirmed the significant overlap (NES=1.23; **SF. 4A**) between the genes overexpressed during AAI (**Fig. 2D**) and those induced upon exposure to IL-13 (**Fig. 3B-C**). Common differentially expressed genes (DEGs) include *Npy1r*, *Serpina3i*, and *Grp* and support IL-13 as one of the main drivers of AAI-induced airway nociceptor neurons transcriptome reprogramming.

We subsequently aimed to delineate the mechanisms by which IL-13 activates nociceptor neurons and changes their transcriptome. First, we used our transcriptomic profiles to identify which IL-13 receptors are expressed by nociceptor neurons and found that only the IL4RII subunits *Il4ra* and *Il13ra1* are detected in these cells (**SF. 4B, Supplementary table 5**). *Il13ra1* expression was stronger in nociceptors than in glial cells and was found in inflammatory airway nociceptor cluster NN8 (**Fig. 1E**; **SF. 2I**), along with the signaling mediator *Stat6* (**SF. 2J)**. Since IL4RII detects both IL-4 and IL-13 and signals via STAT6 to regulate immune cell transcription (32), we tested whether a similar mechanism is at play in nociceptor neurons. We found that IL-13 (30min) triggered STAT6 phosphorylation in JNC and DRG neuron cultures (**Fig. 3D-F**). In addition, IL-13-mediated induction of *Npy1r* was prevented by the STAT6 inhibitor AS1517499 as well as by the JAK1/2 inhibitor ruxolutinib (**Fig. 3G**). In the tested conditions, IL-13 did not induce calcium flux in nociceptor neurons (**SF. 4C**), but nevertheless resulted in an increased in *Npy1r* transcript expression in cultured DRG neurons (**SF. 4D**). Notably, IL-13 also induced *Npy1r* in cultured DRG neurons (**SF.4D**)

Using a similar screening approach, we observed that *Bdnf* overexpression was triggered by the neurotrophin BDNF itself **(SF. 4E),** while *Sting1* was induced by various cytokines **(SF. 4F).** IL-1β led to strong *Il6* overexpression (**Fig. 4A**). While neuronal expression of *Il6* has been reported in other types of neurons (33), the expression of this cytokine has not yet been evidenced in JNC nociceptor neurons. Along with the transcription changes that we elucidated here, we confirmed that IL-6 is expressed and released by IL-1β-exposed JNC neurons (**Fig. 4B-D)**, with levels comparable to IL-1β-exposed splenocytes (**Fig. 4D-E)**.

Since the optogenetic activation of $NPY1R^+$ JNC neurons trigger expiratory reflexes in mice (1) and NPY1R activation impacts pain and itching reflexes (34-42), we sought to test how it would impact airway nociceptor neuron function. Interestingly, we found that along with airway inflammation (**Fig. 5B**), allergen challenges (day 18) significantly increased the levels of the NPY1R ligand NPY in BALF (**Fig. 5C**) and serum (**Fig. 5D**). Of note, NPY levels were normal upon allergen sensitization (day 1 and 7), and while immune cells were still elevated, the neuropeptide concentration returned to baseline during the resolution phase (day 21; **Fig. 5C-D).** A similar pattern was observed for the BALF IL-13 level (**Fig. 5C**). In the lung, *Npy* RNA increased after allergen challenges and remained elevated during the resolution phase, a pattern comparable to the one of the asthma markers *Muc5ac* and *Il13* (**Fig. 5E**). Finally, *Npy1r* overexpression in JNC nociceptors also transiently peaked upon allergen challenges (**Fig. 5F**). We then tested whether these changes were specific to OVA-induced airway inflammation and found a similar rise in BALF NPY in the house dust mite (HDM) model of asthma (**Fig. 5F**). Along with a higher level of BALF immune cells, NPY release was exacerbated in female mice (**Fig. 5H-I**).

We then used the $Na_V1.8^{cre}$::$tdTomato^{fl/wt}$ nociceptor neuron reporter mice and generated lung cryosections as a mean to identify the source of NPY within the airways. Our data showed that NPY expression was restricted to nerve fibers (**Fig. 6A-B, SF. 5A-B**). Around the lung bronchioles, the NPY-expressing neuron fibers were mostly distinct from $Na_V1.8$ positive nociceptor nerve endings (**Fig. 6A-C; SF. 5A-C**). Using triple-labeling, we found that NPY-expressing neurons colocalized with the sympathetic neuron marker tyrosine hydroxylase (TH; **Fig. 6A-C, SF. 5A-C**). Thus, approximately 40% of sympathetic neurons in the stellate ganglia (SG) express NPY (**Fig. 6D-F**) which is in sharp contrast with virtually no expression in the JNC neurons (**Fig. 6D-F**). We conclude that NPY released in the airways originates from sympathetic neurons.

Given that both *Npy1r* and NPY levels were elevated during airway inflammation, we tested whether blocking NPY1R would impact OVA-induced AAI. As opposed to previous studies (43), the NPY1R inhibitor BIBO3301

did not impact AAI immune cell infiltration in our model (**SF. 6A**). Similarly, the conditional knock-out of NPY1R on nociceptor neurons ($Na_V1.8^{cre}$::$NPY1R^{fl/fl}$) did not change the number of immune cells in the BALF (**SF. 6B**).

NPY1R is a Gi-coupled receptor (44) and its activation in DRG nociceptor neurons promotes either analgesia or noxious hypersensitivity (34-42). Given this discrepancy we set out to address how NPY-NPY1R modulates cultured JNC nociceptor neuron sensitivity. To do so, we used whole cell patch clamp recording of $NPY1R^+$ JNC nociceptor neurons ($NPY1R^{cre}$::$tdTomato^{fl/wt}$). We measured electrical changes in response to the NPY1R-specific agonist $Leu^{31}Pro^{34}NPY$. We observed a significant reduction in the nociceptor neurons' excitability (**Fig. 7A-D**), as measured by a reduced number of action potentials in response to current injection. The neurons' activation threshold and the shape of the action potentials were not affected (**Fig. 7E**, **SF. 7A-D**) We also measured a reduced level of intracellular cAMP in cultured JNC neurons exposed to $Leu^{31}Pro^{34}NPY$ (**Fig. 7F**). Notably, $Leu^{31}Pro^{34}NPY$ did not affect TRPA1 and TRPV1 agonist-induced calcium flux **(Fig. 7G**), suggesting that NPY1R blunts nociceptor excitability through other mechanisms, likely involving cAMP.

**DISCUSSION.** Nociceptor neurons shape host defense at mucosal barriers. They do so by detecting environmental danger, triggering an avoidance response, and by tuning immune responses. In the context of allergy, nociceptor neurons were found to amplify dermatitis (10, 15, 16, 45), conjunctivitis (46) and airway inflammation (14, 22, 27, 28, 47, 48). In the lungs, these responses range from coughing and bronchoconstriction to mucus secretion and, depending on the context, amplifying, or taming immunity. Such broad responses are made possible by the highly heterogeneous nature of nociceptor neurons.

Airway nociceptors. The exact neuronal subset involved in these responses remained to be defined. Zhao and colleagues (7) posit that the variety of organs innervated by the vagus nerve explains in part the need for JNC sensory neuron heterogeneity. As such, airway sensory neurons (8, 49) were classified as i) low-threshold stretch-sensitive neurons (essential to the respiratory cycle); ii) mechanoreceptors (sensitive to punctate mechanical stimuli); and iii) high threshold thermosensitive and chemosensitive nociceptors (recruited in response to tissue injury, inflammation, noxious chemicals or temperatures).

Using a combination of lineage reporters, retrograde tracing and transcriptomic analysis, we revealed that JNC airway nociceptor neurons have a unique gene signature segregated from that of other visceral nociceptors (**supplementary table 1**). We identified a new class of *Kcng1*-expressing inflammatory nociceptors (*Trpa1*$^+$, *Trpv1*$^+$, *Il6*$^+$, *Npy1r*$^+$, *IL13ra1*$^+$) that exclusively innervate the airways (NN8). This confirms the assumption of Kupari and colleagues (2) that this neuron subtype (which they label as NG14) consists of pulmonary afferent unmyelinated neurons. Additionally, we found that the airways are preferentially innervated by a neuronal subset (*Kcnv1*$^+$, *Piezo1*$^+$, *Piezo2*$^+$) reminiscent of cough mechanoreceptors (NN7, NG3 in Kupari et al.'s study) as well as by a subset of polymodal nociceptors (NN2), and an $Nav1.8^{low}$ population possibly belonging to the low-threshold stretch-sensitive neurons (25, 49).

AAI reprogramming. We further found a drastic reprogramming of airway nociceptor neurons in response to allergic airway inflammation. Interestingly, the gene signature that we identified largely overlap with the one typically observed in injured nociceptor neurons. These changes are reminiscent of those observed in LPS-exposed airway nociceptor neurons (50). Such similarities may be explained by the neuronal response to cytokines and mediators released in both inflammation and nerve injury models.

While immune and glial cell activation or infiltration is sometimes reported in the spinal cord or DRG following peripheral inflammation or nerve injury (40, 51-55), this was not the case in the JNC of AAI mice. This implies that the neuro-immune interactions occur at the peripheral nerve ending level rather than in the ganglia. Additionally, the nociceptor neurons innervating other organs were shielded from the transcriptional changes we observed in airway neurons. This is in line with the limited systemic inflammation present during AAI.

Cytokines reprograms nociceptor neurons. As we found that AAI reprogrammed airway nociceptor neurons' transcriptome, we tested how various cytokines impact JNC neuron expression profiles. Interestingly, nociceptor neurons showed different gene signatures when exposed to IL-13/IL-4, IL-1β/TNF-α, or BDNF. Thus, it appears that the combination of signaling induced by nerve ending damage, inflammatory cytokines and neurotrophins add up *in vivo* to induce the AAI signature in nociceptors. These findings are also indicative of nociceptor neurons' plasticity to various inflammatory conditions and subsequent context-dependent neuro-immune responses (56).

IL-13 mimics some of the transcriptional changes observed during AAI, an effect that involves STAT6 phosphorylation and subsequent regulation of gene expression. In physiology, our findings suggest that IL-4/IL-13 released by airway $T_H2$ and ILC2 cells are locally sensed by IL4RII-expressing vagal nerve endings. In turn, the intracellular signals are likely to be retrogradely transported to the soma to generate transcriptional changes. Such retrograde transport has been reported in nociceptors for STAT3 (57-60) and CREB (61, 62), and thus may also occur for STAT6.

IL-4 and IL-13 were previously found to induce calcium flux in dorsal root ganglia nociceptor neurons and to trigger an itching reflex (10). While we did not observe direct calcium flux in JNC nociceptor neurons exposed to IL-13, our data converge regarding the functional expression of IL4RII and JAK1/2 activation in nociceptor neurons (63, 64). IL-13/IL-4/JAK/STAT6 is a key signaling pathway essential to type 2 inflammation and allergies (65, 66), and strategies to target it have proven effective to treat atopic dermatitis, asthma and to prevent itching (67). We can reason that the sensory relief observed in these patients may, in part, be due to the silencing of this pathway in nociceptor neurons.

*IL-6*. IL-6 is a pleiotropic cytokine released by a variety of immune cells (68). Its release is enhanced in asthmatic patients (69), various mouse models of asthma (70) and other models of lung inflammation. IL-6 has a variety of immunomodulatory actions, such as inducing $T_H2$ and $T_H17$ differentiation (71, 72), suppressing $T_H1$ (73), inhibiting Tregs (74, 75), or increasing lung fibrosis (76) and mucus secretion (70). IL-6 expression was previously reported in enteric neurons (33), and sometimes appears in sensory neurons' transcriptome following nerve injury (77).

Here, we present the first evidence that IL-6 is expressed and released by JNC nociceptors. We found this release to be enhanced by IL-1β stimulation. This finding likely has important physiological consequences, since the amount released by nociceptor neurons was equivalent to that produced by immune cells from the spleen. Since *Il6* expression is increased in airway nociceptors during AAI, it will be of interest to investigate the contribution of vagal nociceptor-released IL-6 to airway inflammation and define which tissue and cells it targets.

*NPY, NPY1R, pain and allergy*. Pain warns the organism of environmental dangers. Endogenous neuromodulatory mediators can either increase or decrease the organism's perception. In the context of pain, the impact of NPY and NPY1R remains controversial. Nevertheless, a consensus has emerged as for NPY1R expression and antinociceptive effect in the central nervous system (34-37, 39).

The effect on primary afferent nociceptor neurons is less established and NPY exerts a complex influence on pain sensitivity and neuropeptide release. This duality is likely explained by nociceptor neurons' co-expression of NPY1R and NPY2R, with the former dampening pain and inflammation while the latter exacerbates it (38, 40-42). Building on these findings, we presented the first set of data suggesting the impact of NPY-NPY1R on vagal neuron sensitivity. We discovered that NPY-NPY1R decreased JNC nociceptor neuron activity by decreasing the levels of cAMP and reducing action potential firing. cAMP has long been recognized as an intracellular messenger promoting nociceptor sensitization (78-83), an effect mediated in part by PKA-induced phosphorylation of $Na_V1.8$ channels (84).

NPY also fulfills numerous physiological functions, ranging from the control of hunger/feeding to energy homeostasis (85, 86), vasoconstriction (87) and immunomodulation (88). As we found to be the case in our OVA- and HDM-challenged mice, other studies showed elevated NPY levels in various rodent models of lung inflammation (43, 89-92) as well as in the plasma of elderly asthma patients (93). While NPY1R was reported as a driver of lung immune cell infiltration (43), we failed to see any such effect. However, airway NPY was also reported to increase methacholine-induced bronchoconstriction (43, 89), and $NPY1R^+$ vagal neurons were shown to trigger expiratory reflexes (1). It would thus be of interest to assess whether this GPCR expression on vagal neurons is involved in cough and bronchoconstriction.

*Conclusion*. In summary, our data revealed a new class of vagal airway specific nociceptors that acquire an inflammatory gene signature during allergic inflammation or when stimulated with IL-13 and IL-1β. *Npy1r* overexpression was induced by IL-13 in a JAK/STAT6-dependent manner. During allergic airway inflammation, sympathetic nerve fibers, found in proximity to nociceptor fibers within the bronchi, release NPY, which subsequently decrease nociceptor neurons' activity (**Fig. 8**). Future work will reveal whether targeting vagal NPY1R constitutes a relevant therapeutic target to quell asthma-induced bronchoconstriction and cough.

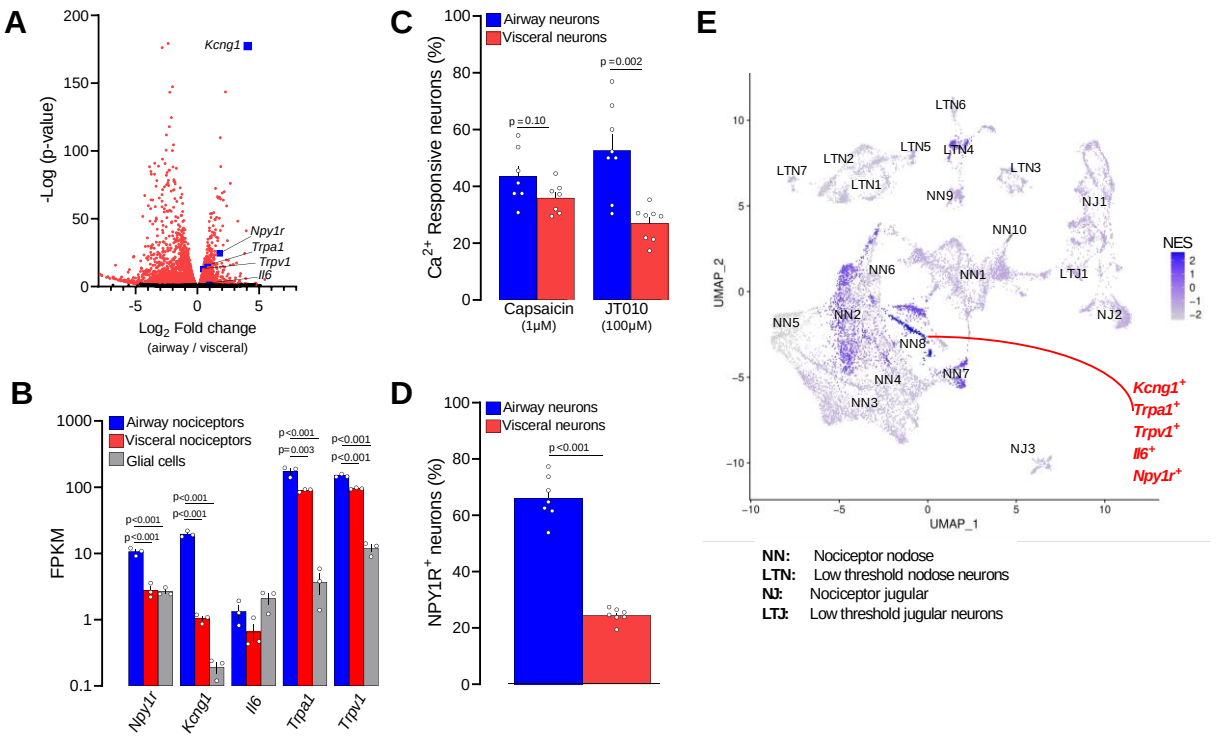


**Figure 1**. Airway vagal nociceptor neurons have a unique molecular profile

**(A-B)** To identify airway-innervating nociceptor neurons, naive 8-week-old male and female nociceptor neurons reporter ($Na_V1.8^{cre}$::$tdTomato^{fl/wt}$) mice were injected intranasally with the retrograde tracer DiD' (200 µM). Fourteen days later, the mice were euthanized and their JNC ganglia isolated and dissociated. Airway-innervating nociceptor neurons ($Na_V1.8^+DiD^+$), visceral nociceptors ($Na_V1.8^+DiD^-$) and glial cells ($Na_V1.8^-$) were purified by flow cytometry and their RNA sequenced. A volcano plot of pairwise comparison of airway-innervating nociceptor neurons versus visceral nociceptor neurons shows differentially expressed transcripts in red (adjusted p-value <0.2). Among others, *Npy1r, Kcng1, Trpa1, Trpv1* and *Il6* were enriched in airway-innervating nociceptor neurons (**A**). *Npy1r*, *Kcng1*, *Trpa1* and *Trpv1* were also more expressed in airway nociceptors when compared to glial cells (**B**).

**(C)** 8-week-old male and female C57BL6 mice were injected intranasally with the retrograde tracer DiD' (200µM). Fourteen days later, the mice were euthanized and their JNC ganglia isolated and dissociated. JNC neurons were cultured (16h) and responsiveness to noxious stimuli was assessed. While responsiveness to the TRPV1 agonist capsaicin (300 nM) was stable between the two groups, the proportion of neurons responsive to the TRPA1 agonist JT010 (50 µM) was higher in airway-innervating neurons ($DiD^+$; **C**).

(**D**) Naive 8-week-old male and female NPY1R reporter ($NPY1R^{cre}$::$tdTomato^{fl/wt}$) mice were injected intranasally with the retrograde tracer DID' (200 µM). Fourteen days later, the mice were euthanized and their JNC ganglia isolated and dissociated. JNC neurons were cultured (16h), and neurons defined by KCl calcium responses. Using fluorescent imaging, we found that NPY1R-expressing neurons ($tdTomato^+$) are more frequent in the airway-innervating population ($DiD^+$; **D**).

**(E)** UMAP of *Slc17a6*$^+$ (VGLUT2) JNC neurons from single-cell RNA sequencing revealed heterogeneous neuronal subsets. Gene set enrichment analysis was performed to address which neuron subtype preferentially innervated the airways, with normalized enrichment score (NES) indicated in blue. The neuronal cluster NN8 expresses several neuro-inflammatory markers (*Il6, Kcng1, Npy1r, Trpa1, Trpv1*) and exclusively innervates the airways (NES=2.3). Experimental details were defined in *Prescott et al.* and the bioinformatic analysis is described in the method section (**E**).

*Data are shown as a representative volcano plot displaying DESeq2 normalized count fold change and nominal p-values for each gene **(A)**, as mean ± S.E.M (**B-D**), or as normalized enrichment score (**E**). N are as follows:*

***a-b**: n=3 biological replicates (4 mice per sample), **c-d**: n=7–8 dishes per group. P-values were determined by DESeq2 analysis (**a**); one-way ANOVA with **post hoc Tukey's** (**b**); or two-sided unpaired Student's t-test (**c, d**). P-values are shown in the figure.*

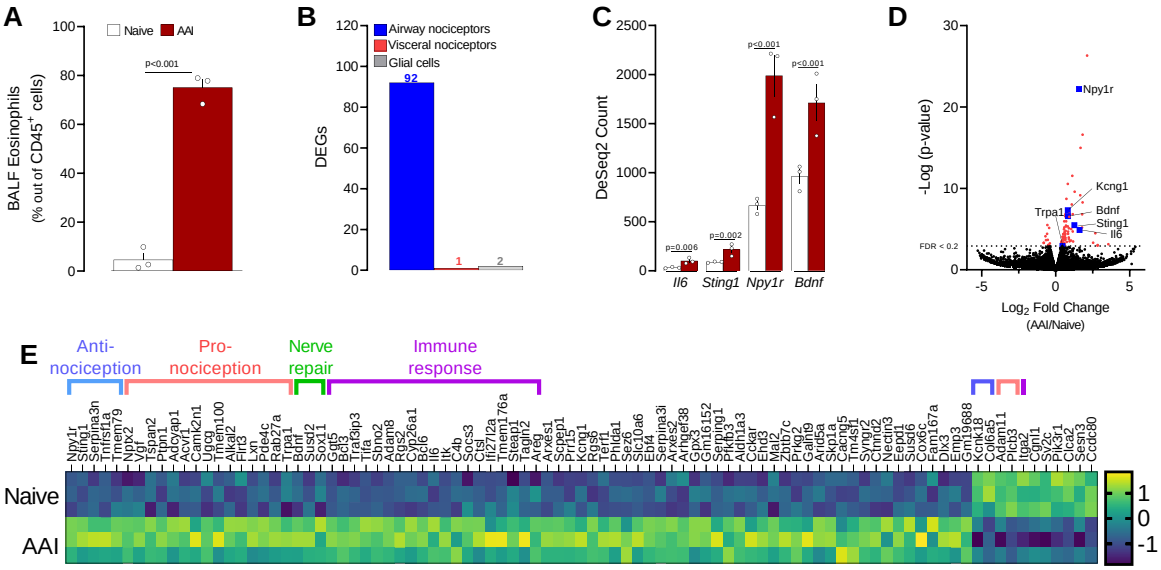


**Figure 2**. Allergic airway inflammation reprograms airway nociceptors transcriptome.

(**A**) 8-week-old male and female nociceptor neuron reporter (Nav1.8$^{cre}$::tdTomato$^{fl/wt}$) mice underwent the ovalbumin mouse models of asthma. Allergic inflammation was induced in mice by an initial sensitization to ovalbumin (OVA) (i.p. day 0 and 7) followed by inhaled OVA challenges (days 14-17). One day after the last allergen challenge, the bronchoalveolar lavage fluid (BALF) was harvested and immunophenotyped by flow cytometry. OVA-exposed mice showed significant airway inflammation characterized by a significant eosinophilic (CD45$^{+}$CD11C$^{low}$SiglecF$^{Hi}$) infiltration (**A**).

(**B-E)** To identify airway-innervating nociceptor neurons, naive 8-week-old male and female nociceptor neuron reporter mice (Na$_V$1.8$^{cre}$::tdTomato$^{fl/wt}$) were injected intranasally with the retrograde tracer DiD' (200 µM). Fourteen days later, the mice were euthanized and their JNC ganglia isolated and dissociated. Airway-innervating nociceptor neurons (Na$_V$1.8$^{+}$DiD$^{+}$), visceral nociceptors (Na$_V$1.8$^{+}$DiD$^{-}$) and glial cells (Na$_V$1.8$^{-}$) were purified by flow cytometry and their RNA sequenced. Differentially expressed genes were virtually only observed in airway-innervating nociceptor neurons (**B**). Among others, *Il6, Sting1, Npy1r*, and *Bdnf* were overexpressed in airway-innervating nociceptor neurons (Na$_V$1.8$^{+}$DiD$^{+}$; **C**). Pairwise comparison shows differentially expressed transcripts in airway-innervating nociceptor neurons between naive and AAI conditions, shown as a volcano plot (adjusted p-value <0.2 in red; **D**) and heatmap (**E**). Genes were sorted by putative function based on a literature review (**E**).

*Data are shown as mean ± S.E.M (**A-C**), a volcano plot displaying DESeq2 normalized count fold change and nominal p-values for each gene **(D),** or a heatmap displaying the z-score of DESeq2 normalized counts **(E).** N are as follows: **a-e**: n=3 biological replicates (4 mice per sample). P-values were determined by a two-sided unpaired Student's t-test (**a**) DESeq2 analysis **(**adjusted p-value in **c** and nominal p-value in **d)**. P-values are shown in the figure.*

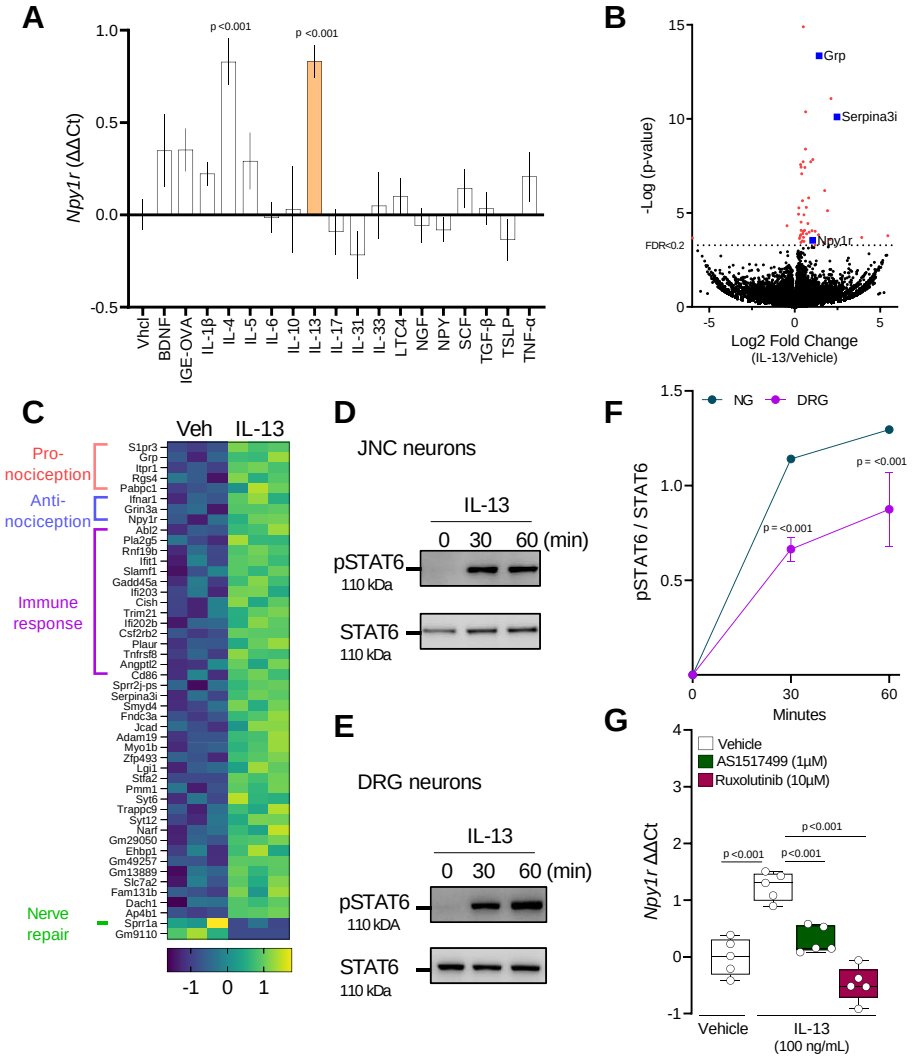


**Figure 3**. IL-13 reprograms nociceptor neurons

(**A**) 8-week-old male and female C57BL6 mice JNC neurons were cultured and exposed (24h) to various inflammatory mediators. Changes in *Npy1r* transcript expression were assessed by qPCR. In comparison to the vehicle, IL-4 and IL-13 (100 ng/mL) increased JNC neurons' expression of *Npy1r*.

(**B-C**) 8-week-old male and female nociceptor neuron reporter ($Na_V1.8^{cre}$::$tdTomato^{fl/wt}$) mice JNC neurons were cultured (24h) with IL-13 or vehicle. The nociceptor neurons were then purified by flow cytometry ($tdTomato^{+}$) and their RNA sequenced. Pairwise comparison shows 48 differentially expressed genes between the vehicle and IL-13 conditions, shown as a volcano plot (adjusted p-value <0.2 in red; **B**) and heatmap (**C**).

(**D-F**) Naive 8-week-old male and female C57BL6 mice JNC or DRG neurons were cultured and exposed (30–60 minutes) to IL-13 (100 ng/mL) or vehicle. Changes to pSTAT6 were analyzed by Western blot. IL-13 time-dependently increased the pSTAT6/STAT6 ratio in DRG (**D, F**) and JNC (**E, F**) neurons.

**(G)** In the presence or absence of the STAT6 inhibitor AS1517499 (1 μM) or the JAK1/2 inhibitor ruxolutinib (10 μM), naive 8-week-old male and female C57BL6 mice JNC neurons were cultured (24h) with IL-13 (100 ng/mL) and changes to *Npy1r* transcript expression was analyzed by qPCR. *Npy1r* overexpression induced by IL-13 was blocked by both AS1517499 and ruxolutinib.

*Data are shown as mean ± S.E.M (**A, F**), as a volcano plot displaying DESeq2 normalized count fold change and nominal p-values for each gene **(B),** as a heatmap displaying the z-score of DESeq2 normalized counts **(C),** as Western blots **(D-E),** or as box (25th–75th percentile) and whisker (min-to-max) plot (**G**). N are as follows: **a**: n=3–4 cultures from different mice per group, **b, c:** n=3 cultures from different mice per group, **d-f**:*

*n=1 JNC culture and n=3 DRG cultures from different mice,* ***g****: n=5 cultures from different mice per group. P-values were determined by one-way ANOVA with post hoc Dunnett's (****a, f, g****) or DESeq2 analysis (****b****). P-values are shown in the figure or indicated by * for p ≤ 0.05; ** for p ≤ 0.01; *** for p ≤ 0.001.*

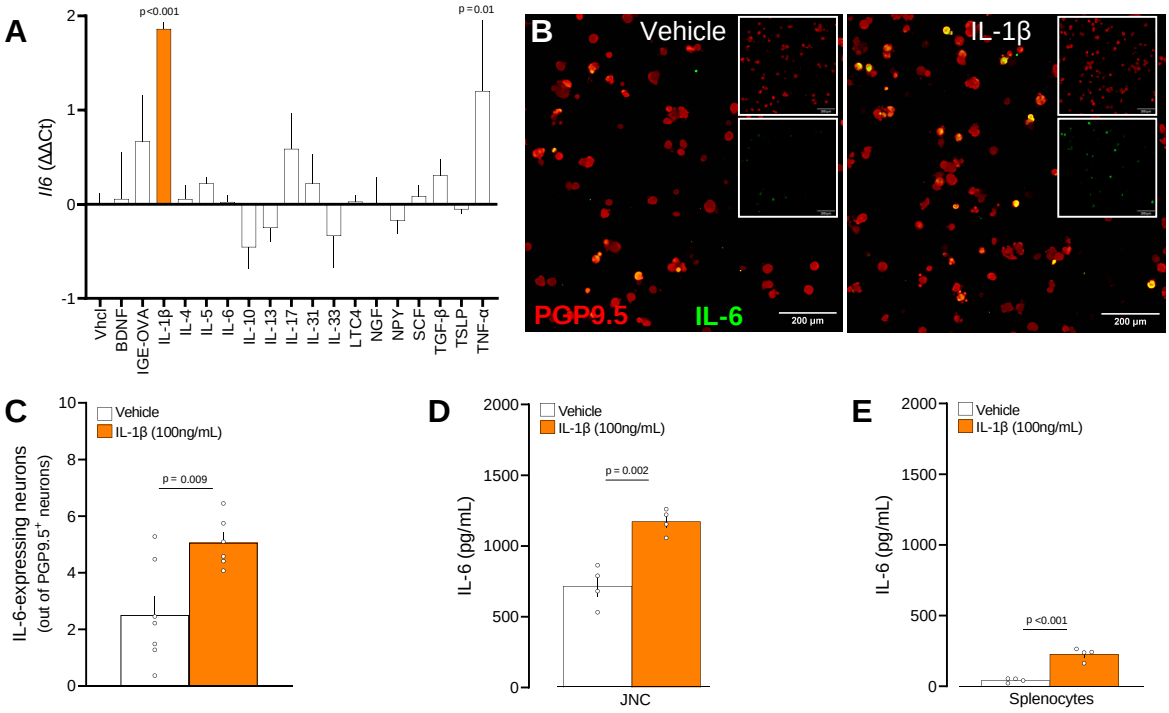


**Figure 4**. JNC nociceptor neurons release IL-6.

(**A**) 8-week-old male and female C57BL6 mice JNC neurons were cultured and exposed (24h) to various inflammatory mediators. Changes in *Il6* transcript expression were assessed by qPCR. In comparison to the vehicle, IL-1β and TNF-α (100 ng/mL) increased JNC neurons' expression of *Il6*.

(**B-C**) IL-6 expression was assessed using immunofluorescence in 8-week-old male and female C57BL6 mice JNC neurons cultures exposed to IL-1β (100 ng/mL; 24h). IL-6 (green) was found to be expressed in PGP9.5+ (red) neurons (**B**), at higher levels in IL-1β-treated than in vehicle-treated neurons (**B**, **C**).

**(D)** 1.5 x $10^4$ JNC neurons from naive 8-weeks-old male and female C57BL6 mice were cultured (36h) in the presence or absence of IL-1β (100ng/mL), and supernatant was harvested for ELISA. In comparison to the vehicle, IL-1β increased IL-6 release by JNC neurons (**C**).

(**E**) 3 x $10^6$ splenocytes from naive 8-weeks-old male and female C57BL6 mice were cultured (36h) in the presence or absence of IL-1β (100ng/mL), and supernatant was harvested for ELISA. In comparison to the vehicle, IL-1β increases IL-6 release by cultured splenocytes (**D**).

*Data are shown as mean ± S.E.M (**A, C-E**) or as cell immunostaining, scale bar 200* µm *(**B**). N are as follows: **a**: n=3–4 cultures from different mice per group, **b-c:** n=6 culture dishes per group, **d-e**: n=4 culture wells per group. P-values were determined by one-way ANOVA with post hoc Dunnett's (**a**) or two-sided unpaired Student's t-test (**c-e**). P-values are shown in the figure.*

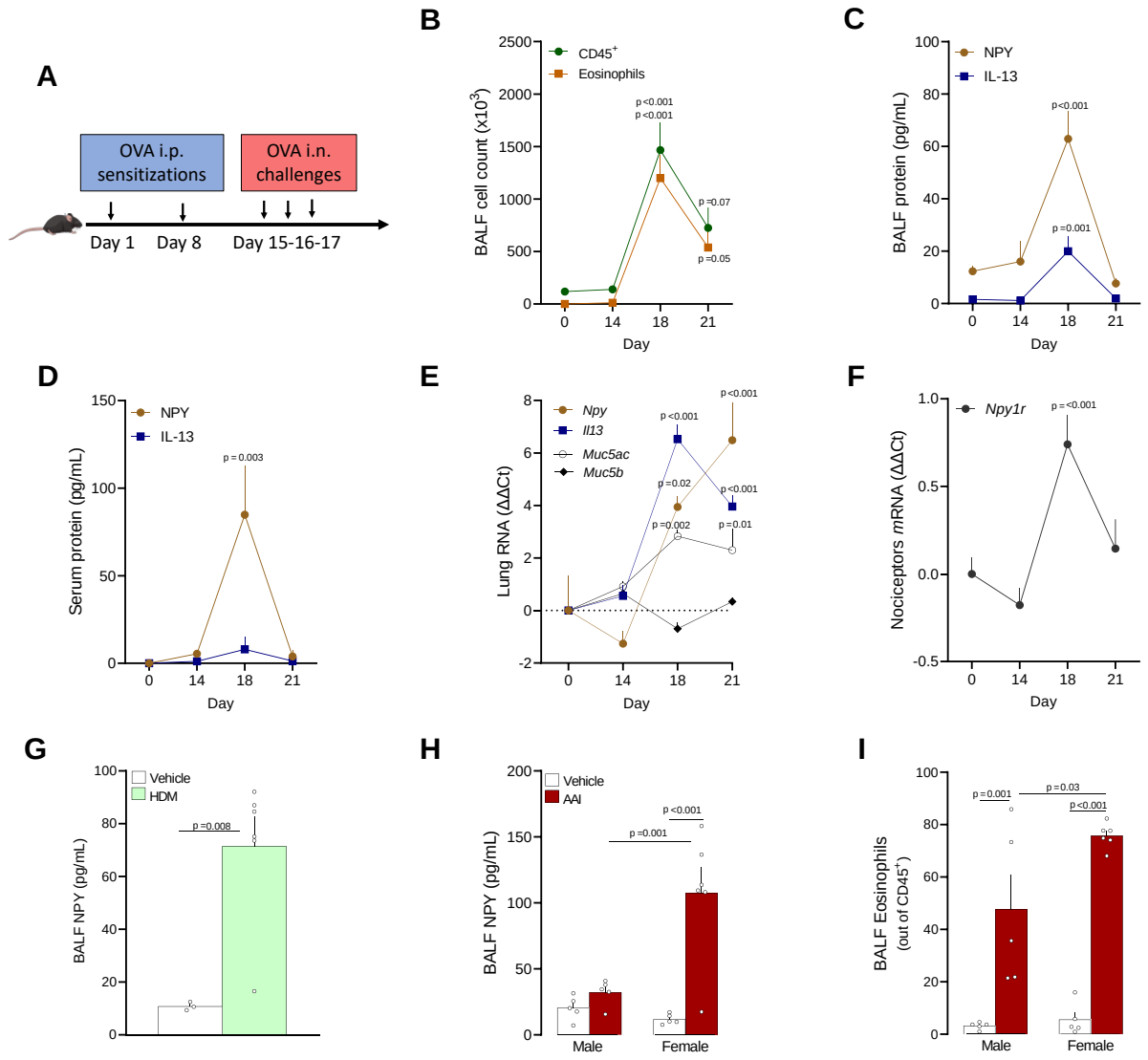


**Figure 5**. NPY is released in airways during allergic airway inflammation

**(A-E)** 8-week-old female C57BL6 mice underwent the ovalbumin mouse models of asthma. Allergic airway inflammation was induced in mice by an initial sensitization to ovalbumin (OVA) (i.p. day 0 and 7) followed by inhaled OVA challenges (i.n. days 14-17). Inflammation typically peaks on day 18 and resolves by day 21. Schematic of the AAI protocol (**A**). BALF, serum and lung were harvested at different time points (days 0, 14, 18, and 21) and the levels of inflammatory mediators were analyzed by ELISAs and qPCR. OVA-exposed mice showed significant airway inflammation characterized by leukocytes ($CD45^+$) and eosinophil ($CD45^+CD11C^{low}SiglecF^{Hi}$) infiltration on day 18 (**B**). Along with this rise in airway inflammation, we found an increase in BALF (**C**) and serum (**D**) NPY, while lung *Npy* expression was also increased (**E**).

(**F**) JNC ganglia were harvested from OVA-exposed nociceptor reporter mice ($TRPV1^{cre}$::$tdTomato^{fl/wt}$), $TRPV1^+$ neurons were purified ($tdTomato^+$) by flow cytometry, and changes to transcript expression were measured by qPCR. At the peak of inflammation (day 18), we found a transient increase in *Npy1r* expression (**F**).

(**G**) To induce allergic airway inflammation, 8-weeks-old female C57BL6 mice were challenged (day 1-5 and 8–10) with house dust mite (HDM; 20µg/50µL, i.n.). The mice were sacrificed on day 11, their BALF harvested, and cell free supernatant analyzed by ELISA. HDM-exposed mice showed a significant increase in BALF NPY level.

**(H-I)** 8-week-old male and female C57BL6 mice underwent the ovalbumin mouse models of asthma. Allergic inflammation was induced in mice by an initial sensitization to ovalbumin (OVA) (i.p. day 0 and 7) followed by inhaled OVA challenges (i.n. days 14-17). Mice were sacrificed on day 18, their BALF harvested; their cells isolated and immunophenotyped by flow cytometry, while BALF supernatant was analyzed by ELISA. NPY levels were enhanced in female mice **(H),** along with a more pronounced immune cell infiltration (**I**).

*Data are shown as experiment schematics (**A**), or as mean ± S.E.M (**B-I**). N are as follows: **b-e**: n=6-7 mice per group, **f**: n=4–10 mice per group, **g:** n= 3–6 mice per group**, h-i:** n= 5–6 mice per group. P-values were determined by one-way ANOVA with post hoc Dunnett's (**b-f,** comparison to day 0); or two-sided unpaired Student's t-test (**g**), or by one-way ANOVA with post hoc Tukey's (**h-i**). P-values are shown in the figure or indicated by * for p ≤ 0.05; ** for p ≤ 0.01; *** for p ≤ 0.001.*

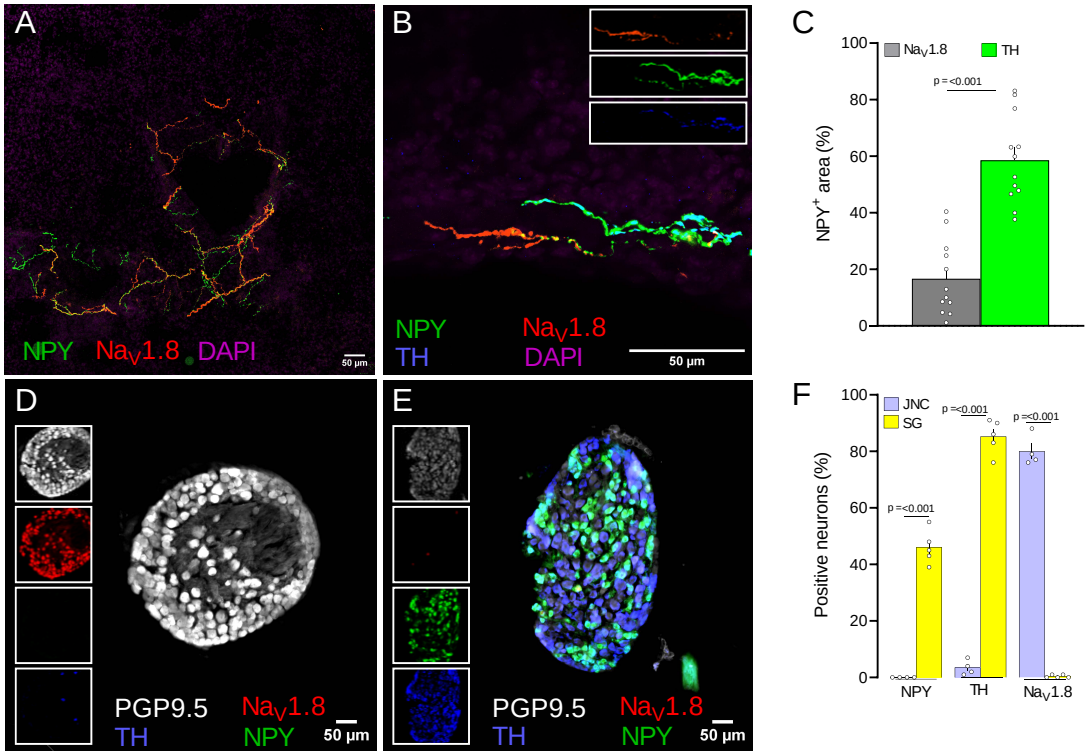


**Figure 6**. NPY is expressed by sympathetic neurons in the lung

**(A-F)** Lung (**A–B**), jugular nodose complex ganglia (JNC; **D**) and stellate ganglia (SG; **E**) were harvested from naïve 8-weeks-old male and female nociceptor neuron reporter ($Na_V1.8^{cre}$::$tdTomato^{fl/wt}$) mice. The tissues were cryosectioned, and the source of NPY assessed by immunofluorescence. In the lung, NPY (green) and $Na_V1.8$ (tdTomato, red) were expressed in nerve fibers around the bronchioles **(A).** While often in proximity, NPY (green) mostly colocalized with the sympathetic neuron marker tyrosine hydroxylase (TH; blue) rather than with $Na_V1.8$ (tdTomato; red) nociceptor fibers **(B-C).** NPY was not expressed in the JNC (**D, F**). In the stellate ganglia (SG), NPY was strongly expressed in $TH^+$ sympathetic neurons (**E, F**). PGP9.5 (white) was used to define JNC and SG neurons (**D, E, F**)

*Data are shown as immunostained tissue, scale bar 50 µm (**A, B, D, E**), or as mean ± S.E.M (**C, F**). N are as follows: **b, c**: n=12 field of views from 4 different mice, **d-f**: n=4–5 mice per group. P-values were determined by a two-sided unpaired Student's t-test (**C, F**). P-values are shown in the figure.*

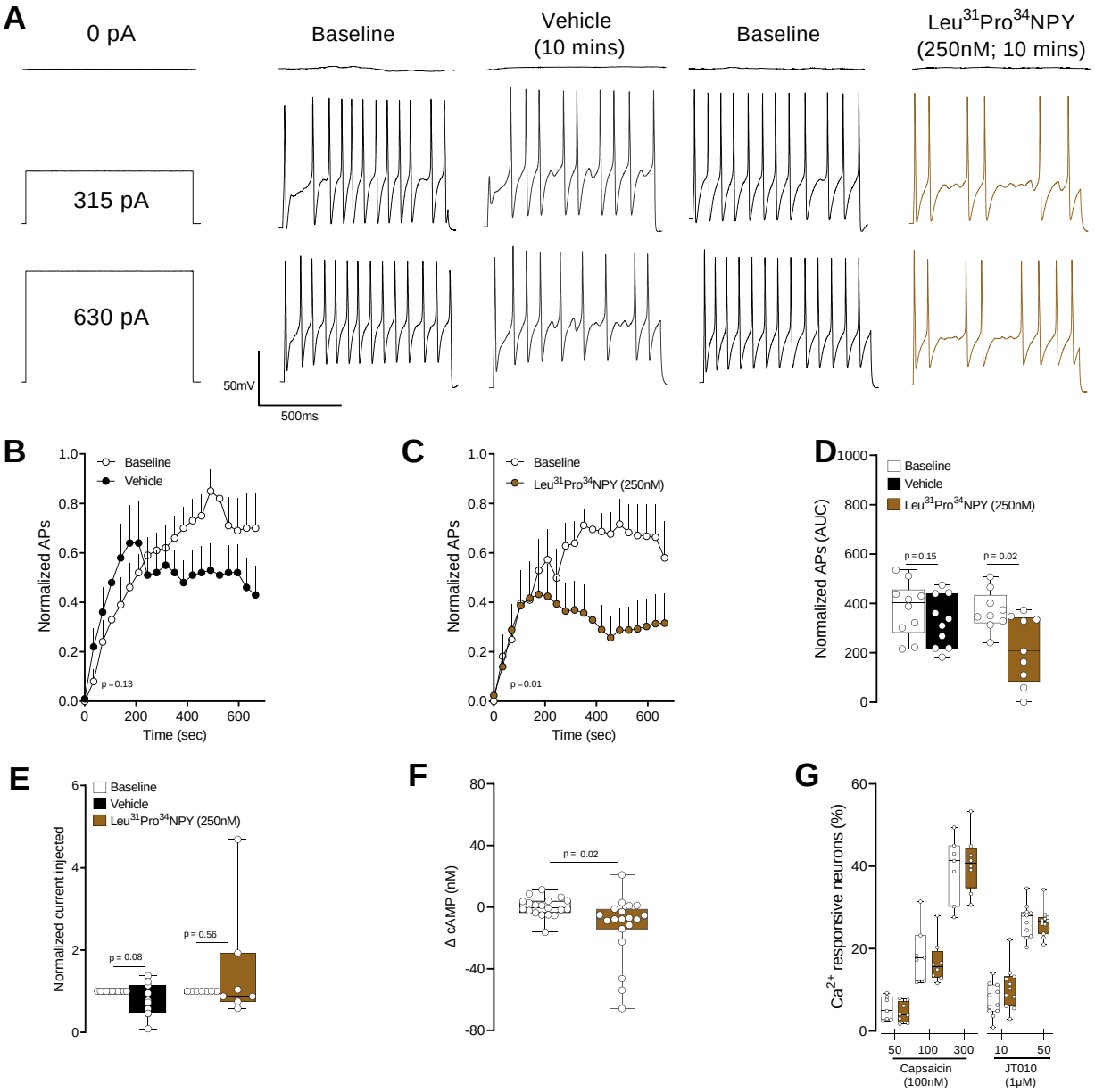


**Figure 7**. NPY1R blunts JNC nociceptors excitability.

**(A-E)** 8-week-old male and female NPY1R reporter (NPY1R$^{cre}$::tdTomato$^{fl/wt}$) mice were sacrificed and their JNC neurons harvested and cultured (16 hours). Whole cell patch clamp electrophysiology was performed on the NPY1R$^{+}$ nociceptor neurons. A current clamp was applied while the neurons' membrane potential was recorded before and after exposing (10 min) the cell to Leu$^{31}$Pro$^{34}$NPY (250 nM) or its vehicle. The number of action potentials for each neuron was normalized by the maximum number observed at baseline (**B-D**). The areas under the curve in **(B)** and **(C)** were calculated and plotted **(D)**. While the vehicle had little to no effect on neuronal excitability (**A**, **B, D**), Leu$^{31}$Pro$^{34}$NPY reduced the number of action potentials in response to current stimulation in NPY1R$^{+}$ (tdTomato) neurons **(A, C, D).** However, the threshold of current required to observe the first action potential was not affected by Leu$^{31}$Pro$^{34}$NPY (250 nM, 10 minutes) as observed in the response to the ramp of current injection **(E).**

**(F)** 8-week-old C57BL6 male and female mice were sacrificed and their JNC neurons harvested and cultured (16 hours). The neurons were exposed to Leu$^{31}$Pro$^{34}$NPY (250 nM) or vehicle for 30 minutes in presence of phosphodiesterase inhibitors. The cells were then lysed and the cAMP concentration assessed by enzymatic assay. Leu$^{31}$Pro$^{34}$NPY significantly reduced cAMP concentration **(F)**.

**(G)** 8-week-old male and female C57BL6 mice were sacrificed and their JNC neurons harvested and cultured (16 hours). The neurons were loaded with the calcium indicator Fura-2AM (5 µM), exposed to $Leu^{31}Pro^{34}NPY$ (250 nM, 5 minutes) or its vehicle and the neurons' responsiveness to noxious stimuli was assessed using calcium microscopy. The calcium responses to the TRPV1 agonist capsaicin (0–300 nM; **G**) or the TRPA1 agonist JT010 (0–50 µM; **F**) were not impacted by $Leu^{31}Pro^{34}NPY$.

*Data are shown as traces of membrane potential for individual neurons (**a**), mean ± S.E.M **(b, c)**, or box (25th–75th percentile) and whisker (min-to-max) plots **(d-g)**. N are as follows: **b, d**: n=10 vehicle treated neurons**, c, d:** n=9 $Leu^{31}Pro^{34}NPY$ treated neurons, **e:** n=7–11 neurons per group, **f**: n=19 culture wells, **g**: n=7–11 culture dishes per group. P-values were determined by two-way ANOVA (**b, c**) or two-sided unpaired Student's t-test **(d-g)**. P-values are shown in the figure.*

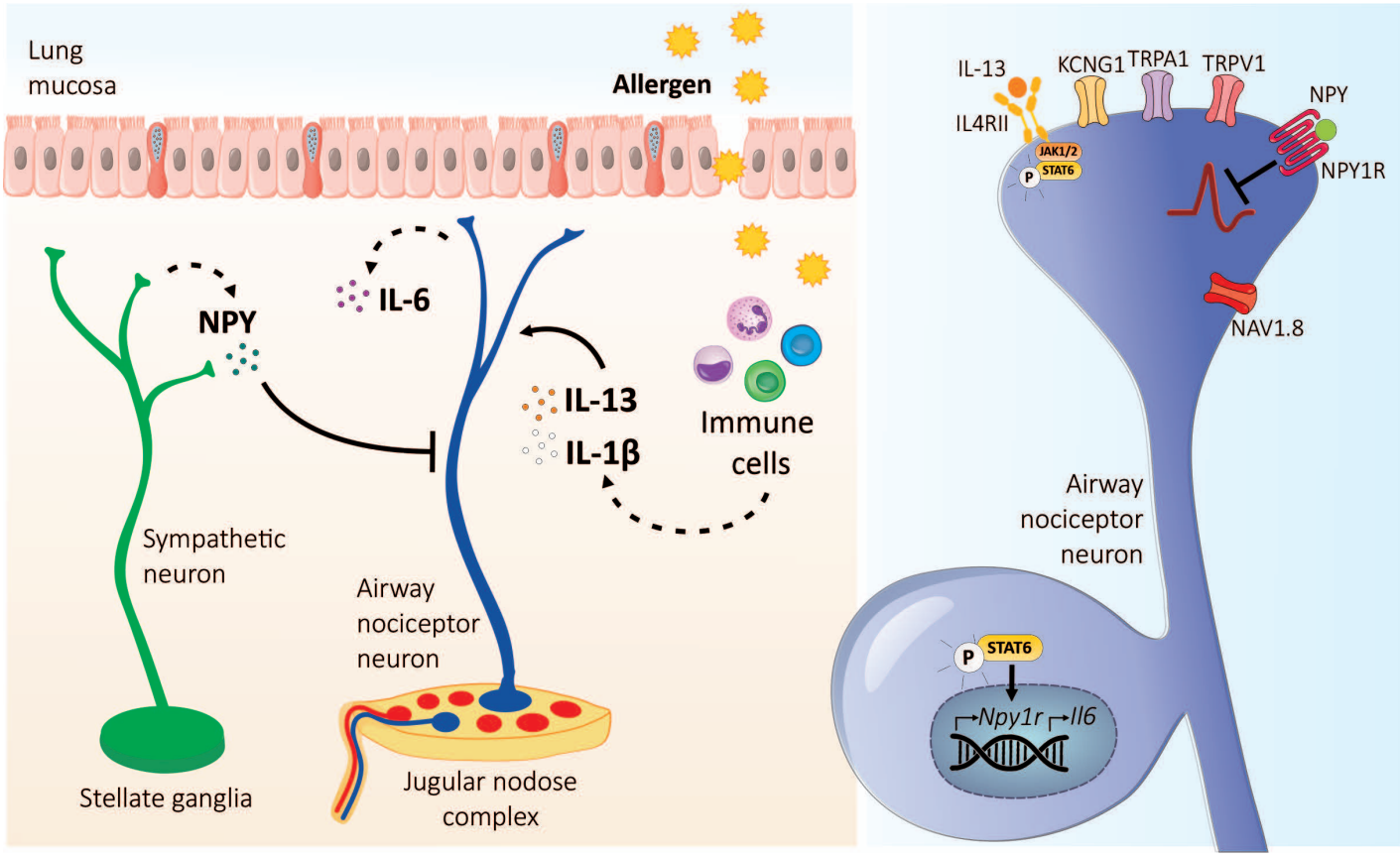


**Figure 8.** IL-13 promotes sensory-sympathetic neurons crosstalk in asthma.

When allergens are present in the airways, the immune and stromal cells in the area become activated and release inflammatory cytokines such as IL-1β and IL-13. These cytokines are then detected by nociceptor neurons, which leads to specific changes in gene expression. For example, exposure to IL-1β increases the expression and release of IL-6 by airway nociceptor neurons. Additionally, IL-13 signaling through its interaction with IL4RII leads to increased expression of Npy1r via phosphorylation of STAT6. Via the action of neuropeptide Y (NPY) released by sympathetic neurons, this cascade ultimately decreased the sensitivity of NPY1R-expressing nociceptor neurons through reduced intracellular levels of cAMP.

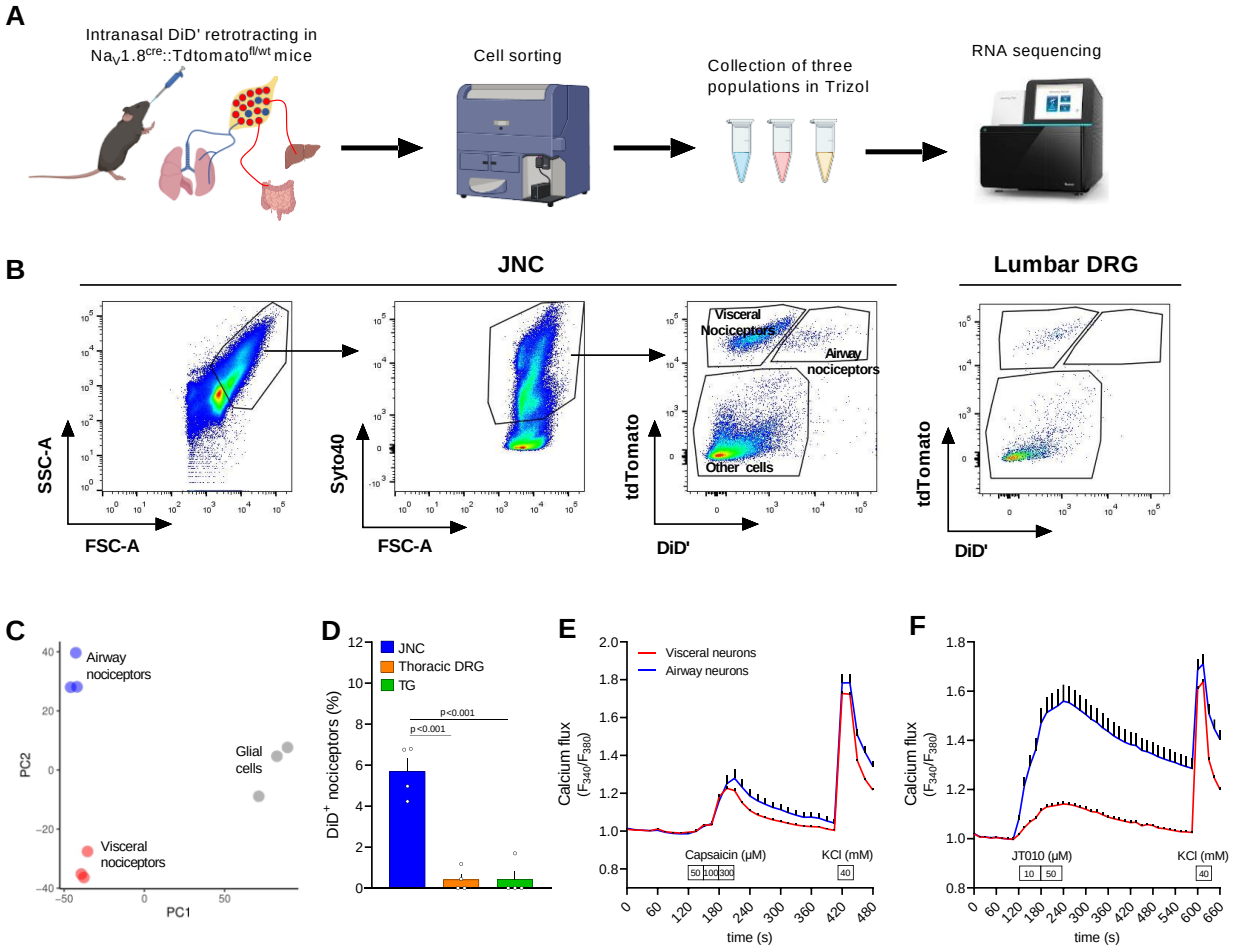


**Supplementary Figure 1.** Airway vagal nociceptor neurons have a unique transcriptome.

**(A)** Diagram depicting the retrotracing of the airway-innervating nociceptor neurons. To identify airway-innervating nociceptor neurons, naive 8-week-old male and female nociceptor neuron reporter ($Na_V1.8^{cre}$::$tdTomato^{fl/wt}$) mice were injected intranasally with the retrograde tracer DID' (200 µM). Fourteen days later, the mice were euthanized and their JNC ganglia isolated, dissociated, and airway nociceptor neurons were purified by flow cytometry. The neurons' transcriptome was then analyzed by RNA sequencing **(A)**.

**(B)** Jugular nodose complex neurons gating strategy. Small debris were eliminated (FSC/SSC), and the whole cells were identified (nucleus marker SYTO40). Populations of airway-innervating nociceptor neurons ($Na_V1.8^+DiD^+$), visceral nociceptors ($Na_V1.8^+DiD^-$) and glial cells ($Na_V1.8^-DiD^-$) were then separated. Lumbar DRG were used as gating controls since they do not innervate the airways **(B)**.

**(C)** The transcriptome of purified airway-innervating nociceptor neurons ($Na_V1.8^+DiD^+$), visceral nociceptors ($Na_V1.8^+DiD^-$) and glial cells ($Na_V1.8^-DiD^-$) was analyzed by RNA sequencing and population segregation was confirmed using principal component analysis **(C)**.

(**D**) Naive 8-week-old male and female $Na_V1.8^{cre}$::$tdTomato^{fl/wt}$ mice were injected intranasally with the retrograde tracer DiD' (200 µM). Fourteen days later, the mice were euthanized and JNC, thoracic DRG, and TG ganglia isolated, dissociated, and imaged with a fluorescence microscope. DiD' retrotracer was detected in JNC nociceptor neurons but virtually absent in other ganglia (**D**).

(**E-F**) Naive 8-week-old male and female C57BL6 mice were injected intranasally with the retrograde tracer DiD' (200 µM). Fourteen days later, the mice were euthanized and their JNC ganglia isolated and dissociated. JNC neurons were cultured (16 h) and calcium responsiveness to noxious stimuli was assessed. While the

average neuronal responsiveness to the TRPV1 agonist capsaicin (300 nM) was stable between the two groups (**E**), the calcium flux induced by the TRPA1 agonist JT010 (50 µM) was higher in airway-innervating nociceptor neurons (**F**).

*Data are shown as a schematic (**A**), flow cytometry dot plot (**B**), principal component analysis (**C**), and mean ± S.E.M (**D–F**). N are as follows: **d**: n=4 culture dishes**, e**: n=116 airway-innervating neurons and 1307 visceral neurons, **f**: n=137 airway-innervating neurons and 1406 visceral neurons. P-values were determined by a two-sided unpaired Student's t-test (**D**) and are indicated in the figure.*

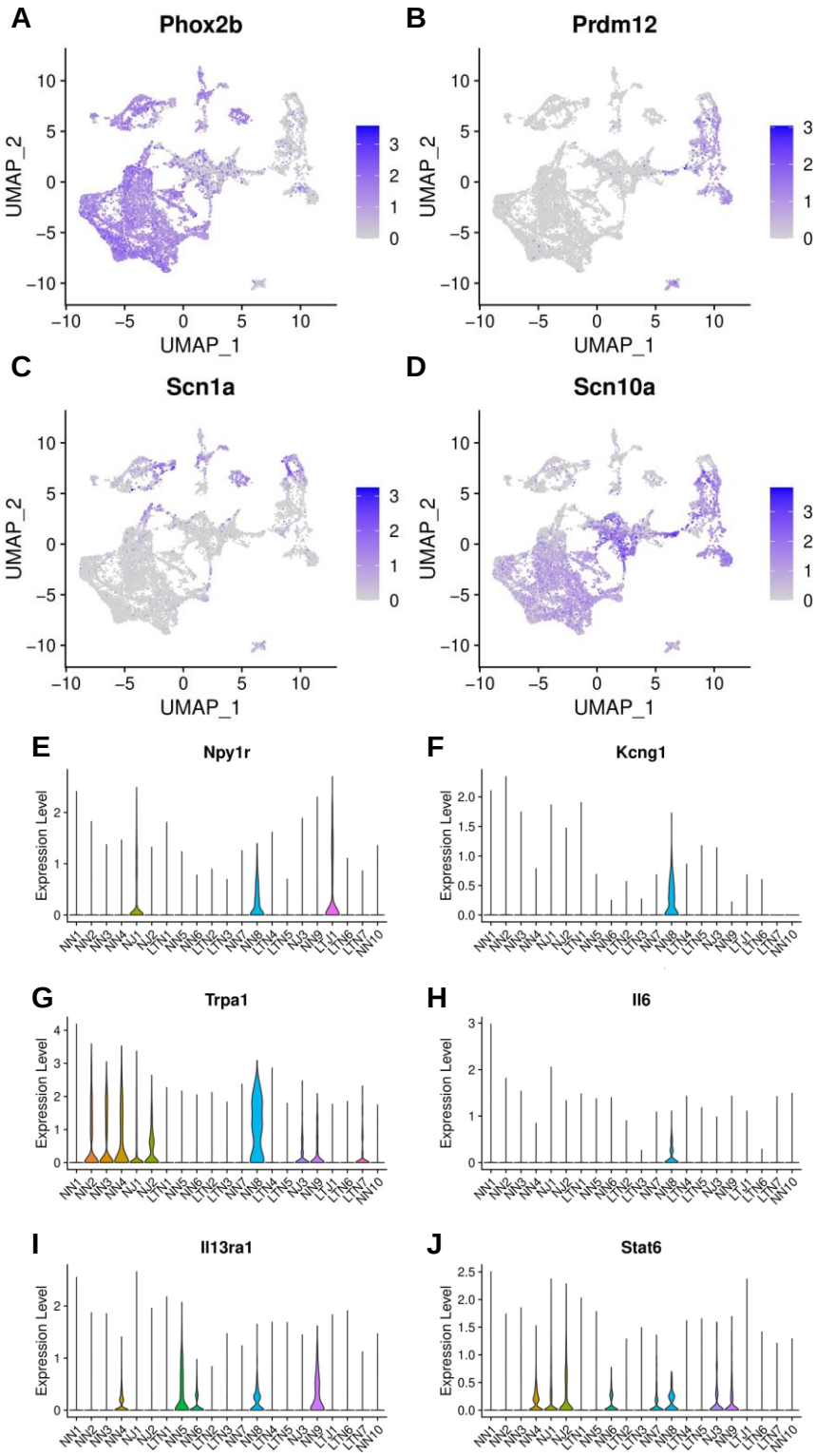


**Supplementary Figure 2.** JNC airway nociceptor neuron markers

(**A-D**) UMAPs of *Slc17a6*$^{+}$ (VGLUT2) JNC neurons from single-cell RNA sequencing showing expression of *Phox2b* (**A**), *Prdm12* (**B**), *Scn1a* (**C**), and *Scn10a* (**D**). *Phox2b* and *Prdm12* delineate the nodose and jugular neurons, while *Scn1a* and *Scn10a* delineate low-threshold sensory neuron and nociceptor neuron populations. The experimental details were defined in *Prescott et al.* and the bioinformatic analysis is described in the methods section (**E**).

(**E–J**) Violin plot showing expression of *Npy1r* (**E**), *Kcng1* (**F**), *Trpa1* (**G**), *Il6* (**H**), *Il13ra1* (**I**), *Stat6* (**J**) in neuronal cells for each cluster identified by single-cell sequencing. All these genes are co-expressed in the airway-specific nociceptor neuron cluster NN8. The experimental details were defined in *Prescott et al.* and the bioinformatic analysis is described in the methods section (**E**).

*Data are shown as UMAPs with log-normalized expression as a feature (Seurat, **A-D**) or as a violin plot of the log-normalized expression (**E-J**).*

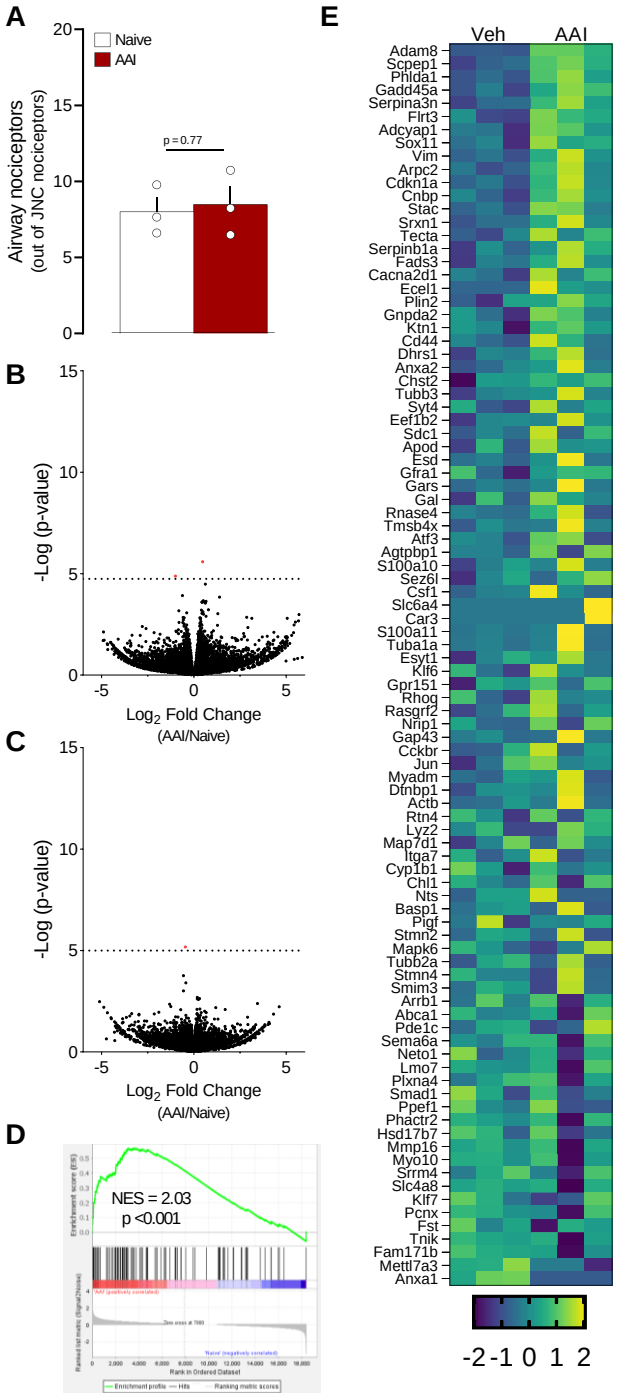


**Supplementary figure 3.** Airway-innervating nociceptor neurons from AAI mice overexpress nerve injury markers

(**A-C**) 8-week-old male and female nociceptor neuron reporter ($Na_V1.8^{cre}$::$tdTomato^{fl/wt}$) mice underwent the ovalbumin mouse models of asthma. Allergic inflammation was induced in mice by an initial sensitization to ovalbumin (OVA) (i.p. day 0 and 7) followed by inhaled OVA challenges (days 14–17). On days 2, 3, and 4, mice were injected intranasally with the retrograde tracer DiD' (200 µM). One day after the last allergen challenge, the mice were euthanized and their JNCs isolated and dissociated, and airway-innervating nociceptor neurons ($Na_V1.8^+DiD^+$) were purified by flow cytometry (**A**). Visceral nociceptor ($Na_V1.8^+DiD^-$) and glial cell ($Na_V1.8^-$) transcriptomes were analyzed by RNA sequencing (**B-C**). The number of JNC airway-innervating nociceptor neurons is similar between naïve and OVA-exposed mice ($tdTomato^+DiD^+$) (**A**). A volcano plot (adjusted p-value <0.2 in red) of pairwise comparison of naive versus AAI visceral nociceptors ($Na_V1.8^+DiD^-$) shows one differentially expressed gene (**B**). A volcano plot (adjusted p-value <0.2 in red) of pairwise comparison of naive versus AAI glial cells ($Na_V1.8^-$) shows two differentially expressed genes (**C**).

(**D–E**) Gene set enrichment analysis showed a strong enrichment of a nerve injury signature(31) (*Adcyap1*, *Adam8*, *Sox11*) (NES=2.03) in airway nociceptor neurons from AAI mice (**D**). The heatmap shows prototypical injured neuron marker gene expression in naïve and AAI mice airway nociceptor neurons (**E**).

*Data are shown as mean ± S.E.M (**A**), a volcano plot displaying DESeq2 normalized count fold change and nominal p-values for each gene **(B, C),** **a** gene set enrichment plot **(D)** or a heatmap displaying the z-score of the DESeq2 normalized counts **(E).** N are as follows: **a–e**: n=3 biological replicates (4 mice per sample). P-values were determined by a two-sided unpaired Student's t-test (**a**), DESeq2 analysis (**b, c**), or GSEA analysis (**d**). P-values are shown in the figure.*

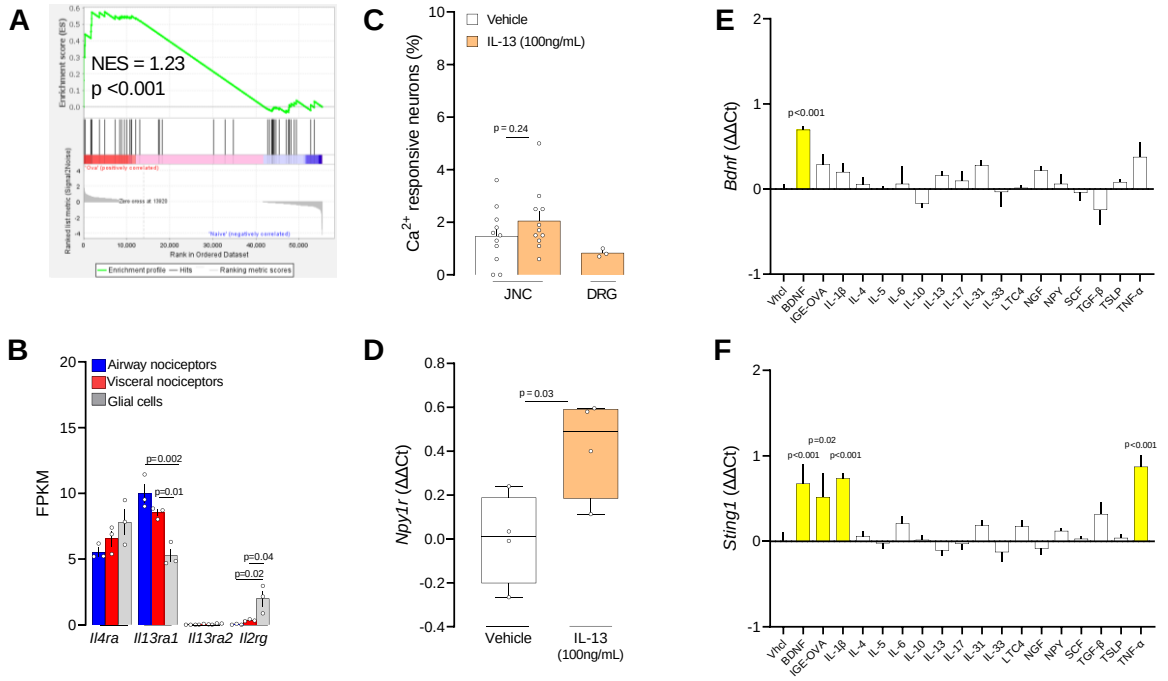


**Supplementary figure 4.** Asthma-driving cytokines reprogram airway nociceptor neurons.

(**A**) DEGs in AAI mice airway-innervating nociceptor neurons and in IL-13-exposed significantly overlap (NES=1.23) (**A**).

(**B**) Naive 8-week-old male and female nociceptor neurons reporter ($Na_V1.8^{cre}$::tdTomato$^{fl/wt}$) mice were injected intranasally with the retrograde tracer DID' (200 µM). Fourteen days later, the mice were euthanized and their JNC ganglia isolated and dissociated. Airway-innervating nociceptor neurons ($Na_V1.8^+DiD^+$), visceral nociceptors ($Na_V1.8^+DiD^-$) and glial cells ($Na_V1.8^-$) were purified by flow cytometry and RNA sequenced. Both IL4RII subunits, *IL4ra* and *IL13ra1*, were detected in JNC nociceptors. Other IL-13 and IL-4 receptors are not detected. *IL13ra1* transcript expression was higher in nociceptor neurons when compared to levels measured in glial cells (**B**).

**(C)** Naive 8-week-old male and female C57Bl6 mice were euthanized and their JNC and DRG ganglia were isolated and cultured (16 h). The neurons were then loaded with the calcium indicator Fura-2AM (5 µM) and their responsiveness to IL-13 (100 ng/mL) was assessed using calcium microscopy. DRG and JNC neurons show limited calcium response when exposed to IL-13 compared to its vehicle **(C)**.

(**D**) Naive 8-week-old male and female C57BL6 mice DRG neurons were isolated and cultured in the presence of IL-13 (100 ng/mL; 24 h) or its vehicle. Transcript levels were assessed by qPCR. In comparison to the vehicle, IL-13 increased DRG neurons' expression of *Npy1r* (**D**).

(**E-F**) *Bdnf* (**E**) and *Sting1* (**F**) transcript levels were assessed by qPCR in 8-week-old male and female C57BL6 mice JNC neuron cultures after exposure to various inflammatory mediators. In comparison to the vehicle, BDNF modulated its own expression in nociceptor neurons (**E**), while IL-1β, BDNF, IgE-OVA and TNFα increased *Sting1* transcript expression (**F**).

*Data are shown as a GSEA enrichment plot **(A)** as mean ± S.E.M (**B-C, E-F**), or as box (25th-75th percentile) and whisker (min-to-max) plots (**D**). N are as follows: **b**: n=3 biological replicates (4 mice per sample), **c**: n=11 culture dishes for JNC and 3 culture dishes for DRG, **d**: n=4 cultures from different mice per group **e-f**: n=3–4 cultures from different mice per group. P-values were determined by GSEA analysis (**A**), one-way ANOVA with post hoc Tukey's (**B**) or post hoc Dunnett's (**E-F**); or a two-sided unpaired Student's t-test (**C-D**). P-values are shown in the figure.*

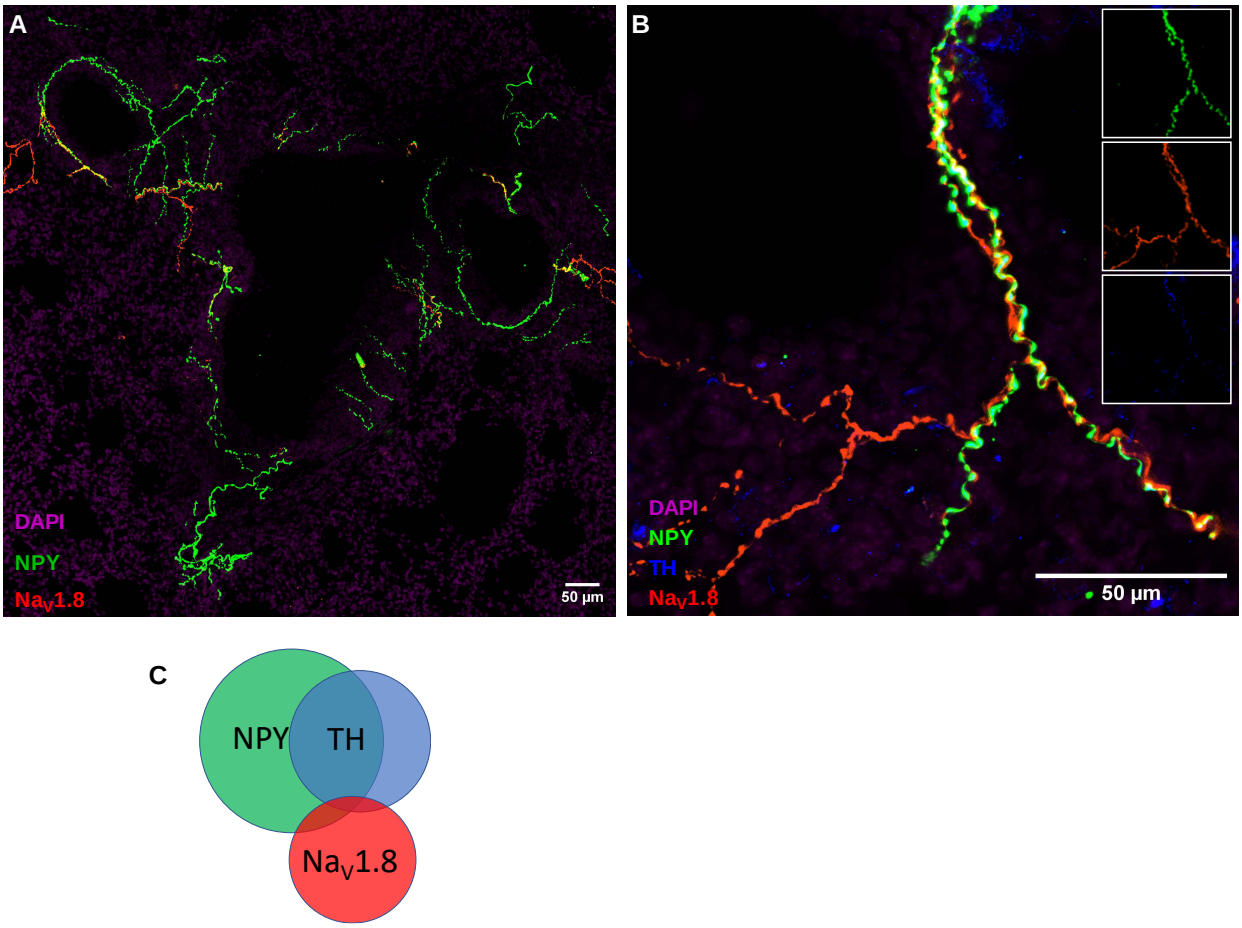


**Supplementary figure 5.** Airway-innervating sympathetic neurons express NPY.

**(A-B)** The lungs of 8-week-old male and female nociceptor neuron reporter (Na$_V$1.8$^{cre}$::tdTomato$^{fl/wt}$) mice were harvested, cryosectioned, and NPY expression was assessed by immunofluorescence. Representative lung images (20x) showed NPY (green), nuclei (purple), and Na$_V$1.8 (red) distribution (**A**). Representative lung images (40x) showed NPY (green), nuclei (purple), Na$_V$1.8 (red), and TH (blue) distribution (**B**) A Venn diagram shows that NPY colocalized with lung TH$^+$ sympathetic fibers, but was largely distinct from Na$_V$1.8$^+$ nociceptors neurons fibers (**C**).

*Data is shown as tissue immunostaining, scale bar = 50µm (**A,B**) or a Venn diagram (**C**). N are as follows: **c**: n=12 field of views from 4 different mice.*

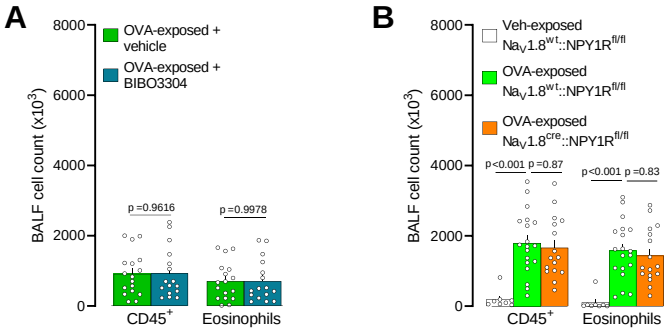


**Supplementary figure 6.** NPY does not impact immune cell infiltration.

(**A**) 8-week-old female C57BL6 mice underwent the ovalbumin mouse models of asthma. Allergic inflammation was induced in mice by an initial sensitization to ovalbumin (OVA) (i.p. day 0 and 7) followed by inhaled OVA challenges (days 14–17). NPY1R blocker BIBO3304 (25 µg/200 µl, i.p.) or its vehicle (DMSO 0.33%) was injected daily (day 13–17). One day after the last allergen challenge, the bronchoalveolar lavage fluid (BALF) was harvested and immunophenotyped by flow cytometry. The NPY1R blockade did not impact leukocytes ($CD45^{+}$) and eosinophils ($CD45^{+}CD11C^{low}SiglecF^{Hi}$) BALF infiltration (**A**).

(**B**) 8-week-old female nociceptor neuron NPY1R conditional knockout ($Nav1.8^{wt}$::$NPY1R^{fl/fl}$) and littermate control mice ($Nav1.8^{wr}$::$NPY1R^{fl/fl}$) underwent the ovalbumin mouse models of asthma. Allergic inflammation was induced in mice by an initial sensitization to ovalbumin (OVA) (i.p. days 0 and 7) followed by inhaled OVA challenges (days 14–17). One day after the last allergen challenge, the bronchoalveolar lavage fluid (BALF) was harvested and immunophenotyped by flow cytometry. OVA-exposed mice showed significant airway inflammation characterized by increased leukocyte ($CD45^{+}$) and eosinophil ($CD45^{+}CD11C^{low}SiglecF^{Hi}$) infiltration, but this parameter was not affected by the conditional KO of NPY1R (**B**).

*Data are shown as mean ± S.E.M (**A-B**). N are as follows: **a**: n=17 mice per group **b**: n=6 (naive) and 16–19 (AAI) mice per group. P-values were determined by a two-sided unpaired Student's t-test (**A**) or one-way ANOVA with post hoc Tukey's (**B**). P-values are shown in the figure.*

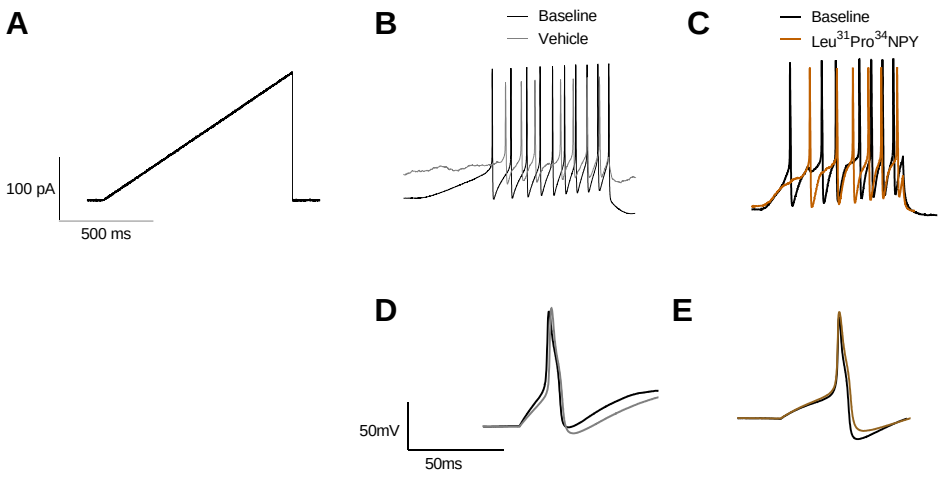


**Supplementary figure 7.** NPY does not impact the nociceptor neuron activation threshold.

**(A-E)** 8-week-old male and female NPY1R reporter (NPY1R$^{cre}$::tdTomato$^{fl/wt}$) mice were sacrificed and their JNC neurons harvested and cultured (16 hours). Whole-cell patch clamp electrophysiology was performed on NPY1R$^{+}$ nociceptor neurons. Current ramps were injected initially from 0 to 100 pA with increasing 100 pA increments while the neurons' membrane potential was recorded before and after exposing (10 min) the cell to Leu$^{31}$Pro$^{34}$NPY (250 nM) or its vehicle. The current injection protocol is depicted in (**A**). The current required to trigger the first action potential was not affected by the vehicle **(B)** nor by treatmenr with Leu$^{31}$Pro$^{34}$NPY. The shape and duration of the action potentials was identical before and after vehicle **(D)** and Leu$^{31}$Pro$^{34}$NPY treatment **(E).**

*Data are shown as traces of membrane potential for individual neurons (**B–E**)*

**Supplementary Table 1.** Airway neuronal subtypes**.** Single-cell sequencing data of JNC cells from Prescott et al. were reanalyzed using Seurat. Neuronal cells were selected based on *Slc17a6* (Vglut2) expression. A total of 21 neuronal populations were identified. *Phox2b* and *Prdm12* were used to identify nodose and jugular groups, while nociceptor neurons and low-threshold sensory neurons were defined based on their expression of *Scn10a* and *Scn1a*. The markers identified for each cluster were compared to airway-innervating neurons sequencing by GSEA. A positive normalized enrichment score indicates preferential innervation of the airways for a given neuronal population. Detailed classification of neurons preferentially innervating the airway is displayed in a tab. Other tabs display the average expression of all genes for all neuronal clusters and DESeq2 analysis comparing airway and visceral nociceptor neurons.

**Supplementary Table 2.** DESeq2 analysis of JNC cell populations in AAI and Naive conditions. 8-week-old male and female nociceptor neuron reporter (Nav1.8$^{cre}$::tdTomato$^{fl/wt}$) mice underwent the ovalbumin mouse models of asthma. Allergic inflammation was induced in mice by an initial sensitization to ovalbumin (OVA) (i.p. days 0 and 7) followed by inhaled OVA challenges (days 14–17). On day 2, 3, and 4, mice were injected intranasally with the retrograde tracer DiD' (200 µM). One day after the last allergen challenge, the JNC neurons were harvested for flow cytometry purification and RNA sequencing. DESeq2 pairwise comparison of airway-innervating (Na$_V$1.8$^+$DiD$^+$) naive nociceptor neurons versus AAI nociceptor neurons counterparts shows 92 differentially expressed genes. A literature review for each gene allowed a classification of their expected function (41, 68, 94-143). Other tabs display DESeq2 analysis of visceral nociceptors (Na$_V$1.8$^+$DiD$^+$) and glial cells (Na$_V$1.8$^-$).

**Supplementary Table 3.** Enrichment of a nerve injury signature in nociceptors during AAI. Data from Cobos and colleagues (31) shows various differentially expressed genes induced in DRG nociceptors three days after nerve injury. This dataset was reanalyzed by DESeq2, and the top 100 genes (Log2FC > 0.5, 100 lowest p-values) induced after nerve injury were selected. The table shows their DESeq2 counts in airway nociceptor neurons from naïve and AAI mice.

**Supplementary Table 4.** DEGs in IL-13 exposed nociceptors. 8-week-old male and female nociceptor neuron reporter (Na$_V$1.8$^{cre}$::tdTomato$^{fl/wt}$) mice JNC neurons were cultured (24 h) with IL-13 (100 ng/mL) or vehicle. The nociceptor neurons were then purified by flow cytometry and changes to their transcriptome analyzed by RNA sequencing. The tables display the results of the DESeq2 analysis comparing the vehicle and IL-13-exposed conditions. DEGs are showed in a separate tab. A literature review for each gene allowed a classification of their expected function(41, 144-166).

**Supplementary Table 5.** FPKM normalized sequencing data. Fragment per kilobase per million (FPKM) normalized values for all sequencing data produced in this study (airway nociceptors, visceral nociceptors, glial cells in naive and allergic airway inflammation conditions, cultured nociceptors exposed to vehicle or IL-13). For all samples, RNA was extracted under identical conditions, and the sequencing performed on the same chip using barcodes.

## METHODS.

**Animals.** Mice were housed in standard environmental conditions (12h light/dark cycle; 23$^o$C; food and water ad libitum) at facilities accredited by CCPA. Parental strain C57BL6 (Jax, #000664), tdTomato$^{fl/fl}$ (Jax, #007908), Trpv1$^{cre/cre}$ (Jax, #017769), Npy1r$^{cre/cre}$ (Jax, #030544) were purchased from Jackson Laboratory. Parental strain Nav1.8$^{cre/cre}$ mice were generously supplied by Prof. John Wood (UCL) and Prof. Rohini Kuner (Heidelberg U). Parental strain NPY1R$^{fl/fl}$ mice were generously supplied by Prof. Herbert Herzog (Gavan Institute of Medical Research). Male and female mice were bred in-house and used between 6 and 12 weeks of age. Cross breeding was used to generate the following genotypes: Na$_V$1.8$^{cre}$::tdTomato$^{fl/wt}$, NPY1R$^{cre}$::tdTomato$^{fl/wt}$, TRPV1$^{cre}$::tdTomato$^{fl/wt}$, Na$_V$1.8$^{cre}$::NPY1R$^{fl/fl}$, and Na$_V$1.8$^{wt}$::NPY1R$^{fl/fl}$ (littermate control).

**Ovalbumin model of allergic airway inflammation.** On days 0 and 7, mice were sensitized by a 200 µl i.p. injections of a solution containing 1 mg/ml ovalbumin (Sigma, #A5503) and 5 mg/ml aluminum hydroxide (Sigma, #

239186). On days 14–17, mice were injected daily with 50 µg/50 µL OVA intranasally. Mice were sacrificed on day 18 unless otherwise indicated.

**House dust mite model of allergic airway inflammation.** Lightly anesthetized (isoflurane 2.5 %, CDMV #108737) mice were challenged (20 µg/50 µL, intranasal) on day 1–5 and 8–10 with house dust mites (CiteQ Biologics, #15J01) and sacrificed on day 11.

**Lung neuron's retrograde tracing.** Mice were injected (50 µL, 200 µM in PBS, 1% DMSO; intranasally) with DiD' (Thermofisher, #D7757) for 3 consecutive days (D2-D4 of OVA protocol). The mice were sacrificed two weeks after the last injection to allow the tracer to reach the JNC.

**BIBO3304:** 30-min prior to the OVA/veh challenges, the mice were injected (25 µg / 200 µL; intraperitoneally) with BIBO3304 (Tocris, #2412) or vehicle (0.2% DMSO diluted in PBS) on days 14, 15, 16 and 17.

**Neuron culture:** Mice were sacrificed and JNC or DRG were dissected into an ice-cold HEPES buffered DMEM medium (Thermofisher, #12430062). JNC ganglia from 2-10 mice were pooled in the same tube. The cells were transferred to a HEPES buffered DMEM medium completed with 1 mg/mL collagenase IV (Sigma, #C5138) + 2.4 U/mL dispase II (Sigma, #04942078001) and incubated for 70 minutes at 37 °C. Ganglia were triturated with glass Pasteur pipettes of decreasing size in DMEM medium, then centrifuged (200 g) over a 15% BSA gradient in PBS to eliminate debris. The neurons were plated on laminin (Sigma, #L2020) coated cell culture dishes. The cells were cultured at 37° with Neurobasal-A medium (Gibco, #21103-049), supplemented with 2% B27 (Thermofisher, #17504044) 0.01 mM AraC (Sigma, #C6645), 200 nM L-Glutamine (VWR, # 02-0131), 100 U/mL penicillin and 100 µg/mL streptomycin (Corning, #30002CI) without neurotrophin unless otherwise indicated. Culture densities and durations are described for each application.

**Cyclic AMP.** JNC neurons were cultured ($1.5x10^3$) in 96 well plates (VWR #10062-900) for 16 hours. The media was removed, and neurons exposed to $Leu^{31}Pro^{34}$NPY (250nM Tocris #1176) or vehicle (PBS containing cAMP phosphodiesterase inhibitor (100 µM Ro-20-1724; Sigma, #557502 and 500 µM 3-Isobutyl-1-methylxanthine; Sigma, #I5879) for 30 minutes. Cells were lysed for enzymatic cAMP measurement assay using a commercial kit and following manufacturer's instructions (Promega, #V1501).

**Calcium microscopy.** C57BL6 or $NPY1R^{cre}$::$tdTomato^{fl/wt}$ DRG or JNC were plated ($2x10^3$) on laminin-coated glass-bottom dishes (35 mm; ibidi, #81218) and cultured overnight. The cells were then loaded with Fura-2-AM (5 µM, 37 °C, Biovision, #125280) for 45min and washed with Standard Extracellular Solution (145 mM NaCl, 5 mM KCl, 2 mM $CaCl_2$, 1 mM $MgCl_2$, 10 mM glucose, 10 mM HEPES, pH 7.5), and imaged at room temperature. Capsaicin 50 nM, 100 nM and 300 nM (Tocris, #0462) or JT010 10 µM and 50 µM (Sigma, #SML1672), or IL-13 (100 ng/mL) were prepared in SES and were flowed (30 seconds, 1 minute and 1 minute, respectively) directly onto neurons using perfusion barrels followed by buffer washout (5 minutes). 40 mM KCl solution was then flowed on the cells for 20 seconds. To test NPY1R effect on neuron sensitivity, $Leu^{31}Pro^{34}$NPY (250 nM; Tocris, #1176) or vehicle was perfused for 5 minutes before the other compounds. A single field of view was acquired per dish. Cells were illuminated by a UV light source (Cool LED, pE-340) with alternating 340 nm and 380 nm excitation, and a camera (Photometrics Prime 95B 25 mm) captured fluorescence emission (515/45 nm) with a 20X objective on a Ti2 microscope (Nikon). Regions of interest (ROI) were manually drawn and 340/380 fluorescence ratios were exported. Microsoft Excel was used for further analysis (Microsoft, USA). Neurons were considered responsive to a compound if the fluorescence ratio increased by at least 10% within 1 minute after injection.

**Electrophysiology.** JNC neurons from $NPY1R^{cre}$::$tdTomato^{fl/wt}$ mice were plated ($2x10^3$) onto Poly-D-lysin and laminin-coated glass-bottom 35 mm dishes (Ibidi #81218) and cultured in supplemented neurobasal medium. TdTomato-positive JNC neurons were identified using a Nikon Eclipse Ti microscope. Whole-cell voltage and current-clamp recordings were performed with an EPC 800 patch clamp amplifier (HEKA) and were filtered at 10 kHz with the internal Bessel filter and digitized using an Axon Instruments Digidata 1440A digitizer at 20 kHz. The neurons were placed in standard external solution (163 mM NaCl, 2.5 mM $CaCl_2$, 2 mM $MgCl_2$, 20 mM glucose, and 10 mM HEPES, pH = 7.4). Recording pipettes were pulled from soda lime glass pipettes (outer diameter 1.5 mm, Kimble® Chase, #41A2502,) using a P-97 microelectrode puller (Sutter Instrument). Pipettes with resistances of 3–5 MΩ were

used for recordings. Pipettes were filled with internal solution (133 mM potassium gluconate, 6 mM NaCl, 1 mM $CaCl_2$, 0.7 mM $MgCl_2$, 10 mM HEPES, and 10 mM EGTA, pH = 7.2, final $K_{in}^+$ concentration –163mM).

For voltage clamp experiments, the neurons were clamped at –60mV. Neuronal currents were recorded before and after drug exposure from a series of depolarization steps ranging from –120 to +70mV in 10 mV intervals. For the current clamp AP protocol, neurons were injected with a series of 35 pA current steps (1 s duration) from 0 to 630 pA. The rheobase protocol involves determining the amount of current injection required to evoke the first AP. In this protocol, a train of 1s depolarizing current ramps were injected initially from 0 to 100 pA with increasing 100 pA increments. These voltage and current clamp experiments were performed before and 10 mins post-addition with a pipette of external solution (vehicle) or $Leu^{31}Pro^{34}$NPY (250 nM; Tocris, #1176). Current amplitudes, APs and rheobase were quantified using Clampfit 10.7 (Molecular Devices). Since baseline activity varied among the JNC neurons, the activity of the neurons after application of vehicle or $Leu^{31}Pro^{34}$NPY was normalized to baseline activity of the same cell.

**Bronchoalveolar lavage fluid (BALF).** Mice were anesthetized by intraperitoneal injection of urethane (250 µL i.p., 20%) and a 20G sterile catheter inserted longitudinally into the trachea. 500 µL followed by 1 mL of ice-cold buffer (PBS, 2% FBS, 1 mM EDTA) containing protease inhibitors (Sigma, #P1860) was injected into the lung, harvested, and stored on ice. BALF underwent a 400g centrifugation (5 min; 4 $^oC$), supernatant of the first flush was harvested and frozen (−80°C) for subsequent ELISA experiments. Cells were resuspended for cell count and flow cytometry analysis.

**BALF immunophenotyping.** Cells were resuspended in red blood cells lysis buffer (Gibco, #A10492-01) for 1 minute then washed with PBS. Cells were then stained with Zombi Aqua (Biolegend, #423102) for 10 minutes, before staining in a flow cytometry buffer (PBS, 2% FBS, 1 mM EDTA) supplemented with 1% Rat Serum. Staining antibodies included anti-CD45–BV421 (1:400; BioLegend, #103134), anti-Siglec-F–PE (1:400; Thermofisher, #12-1702-82), anti-CD11b-APC–Cy7 (1:400, BioLegend, #101262), anti-CD11c–FITC (1:400, BioLegend, #117306), anti-Ly6G–APC (1:400, BioLegend, #127614), anti-Ly6C–PE-Cy7 (1:400, BioLegend #128018), and anti-CD4-PerCP–Cy5.5 (1:400, BioLegend, #116012) for 30 minutes in the dark at 4 °C. $1x10^3$ counting beads (Biolegend, #424902) were added for absolute quantification before data acquisition on a FACS Canto II (BD Biosciences). Leukocytes were gated as $CD45^{pos}$, eosinophils as $CD45^{pos}SiglecF^{high}CD11C^{low}$, alveolar macrophages as $CD45^{pos}SiglecF^{high}CD11C^{high}$, neutrophils as $CD45^{pos}SiglecF^{low}CD11B^{high}LY6G^{high}$, and CD4 T cells as $CD45^{pos}SiglecF^{low}CD11B^{low}CD4^{high}$.

**Flow cytometry sorting of sensory neurons.** $Na_V1.8^{cre}$::$tdTomato^{fl/wt}$ mice were sacrificed and JNC or DRG were dissected into ice-cold HEPES buffered DMEM medium (Thermofisher, #12430062). For RNA sequencing, JNC ganglia were pooled from 4 mice (2 males and 2 females) for each biological replicate. Ganglia were transferred into a HEPES buffered DMEM medium completed with 1 mg/mL collagenase IV (Sigma, #C5138) + 2.4 U/mL dispase II (Sigma, #04942078001) and incubated for 70 minutes at 37°C, then washed in DMEM medium before trituration with glass Pasteur pipettes of decreasing size. Cells were then centrifuged (200g) over a 15% BSA gradient in PBS to eliminate debris. Nucleus were stained with SYTO40 (10 µM, 5 minutes RT; Thermofisher, #S11351) to differentiate cells from axonal debris, washed with PBS, then cells were resuspended in sterile PBS with 2% FBS and filtered (70 µm; VWR, #10204-924).

For DiD'-injected mice, JNC neurons were sorted directly into Trizol (500 µL; Invitrogen, #15596026) and stored at −80°C for subsequent RNA extraction. Airway nociceptors were gated as $Syto40^{hi}tdTomato^{hi}DiD^{pos}$, visceral nociceptors as $Syto40^{hi}tdTomato^{hi}DiD^{lo}$, and glial/stromal $Na_V1.8^-$ cells as $Syto40^{hi}tdTomato^{lo}$.

DiD'-injected mice lumbar DRG neurons and naive $Na_V1.8^{cre}$::$tdTomato^{fl/wt}$ mice JNC neurons were used as gating controls. Naïve mice JNC neurons were used as gating controls for tdTomato.

**ELISA.** Cell free BALF supernatant and serum were used for ELISA quantification after storage at −80°. IL-13 (Thermofisher, #88-7137-88) and NPY (Cusabio, #CSB-E08170M) were measured using commercial kits following manufacturer's instructions.

**Nociceptor neurons ELISA.** C57BL6 mice JNC neurons were cultured ($2x10^3$) in 96 well plates with vehicle or IL-1β (100 ng/mL). After 36 hours, supernatant was harvested, centrifugated (500g) and IL-6 secretion analyzed using a commercial ELISA kit following the manufacturer's instructions (Biolegend, #431304).

**Whole-lung RNA extraction:** RNA was separated from protein and DNA by mixing 500 µL of sample in Trizol with 100 µL chloroform before ultracentrifugation (15 min, 16000g, 4°). The upper phase was mixed with a half volume of 100% isopropanol, transferred to a purification column, and the RNA was then purified using the kit E.Z.N.A. Total RNA Kit I (VWR, #CA101319) following manufacturer's instructions.

**JNC Neurons RNA extraction:** RNA was separated from protein and DNA by mixing 500 µL sample in Trizol with 100 µL chloroform before ultracentrifugation (15 min, 16000g, 4°). The upper phase was mixed with a half-volume of 100° isopropanol, transferred to a purification column, and the RNA purified using the kit PureLink RNA Micro Scale (Thermofisher, #12183016) following manufacturer's instructions.

**Screening of cytokine neuromodulatory capacity.** JNC neurons were plated ($5x10^3$; 200 µL) on laminin-coated 96 well plates and exposed to cytokines (100 ng/mL; IL-1β, IL-4, IL-5, IL-6, IL-10, IL-13, IL-17, IL-31, IL-33, SCF, TGF-β, TSLP or TNF-α), lipid mediators (200 ng/mL; leukotriene C4), neurotrophins (50 ng/mL; nerve growth factor or brain-derived neurotrophic factor), IgE-OVA (10 µg/mL) or NPY (100 nM). Biological replicates were made using different mice preparations for each replicate. After 24 hours of culture, the medium was removed, and the cells harvested in 500 µL Trizol (Thermofisher, #15596018). Samples were then used for RNA extraction and RT-qPCR.

**RT-qPCR**. RNA was reverse transcribed using the SuperScript VILO Master Mix (Thermofisher, #11755250). The cDNA was then subjected to two-step thermocycling using PowerUp qPCR SYBR Green Mix (Invitrogen, #A25742) and data collection was then performed on a Mic qPCR machine (Bio Molecular Systems). 1–3 ng cDNA was used for qPCR from neuron preparations, and 80–100 ng for qPCR from whole lung RNA. Expression levels were normalized using the ΔΔCt method with *Actb* as the reference gene.

The primers used were : *Actb* Forward: TGTCGAGTCGCGTCCACC; *Actb* Reverse: TATCGTCATCCATGGCGAACTGG; *Trpa1* Forward: TCCAAATTTTCCAACAGAAAAGGA; *Trpa1* Reverse: CGCTATTGCTCCACATTGCC; *Npy1r* Forward: CTCGTCCCGCTTCAACAGAG; *Npy1r* Reverse: TCAAAACGGATCAAATCTTCAGCA; *Il6* Forward: GGATACCACTCCCAACAGACC; *Il6* Reverse: AATTGCCATTGCACAACTCTTTTC; *Bdnf* Forward: CAGGTTCGAGAGGTCTGACG; *Bdnf* Reverse: AAGTGTACAAGTCCGCGTCC; *Sting1* Forward: CTGCCGGACACTTGAGGAAA; *Sting1* Reverse: CCGTCTGTGGGTTCTTGGTAG; *Npy* Forward: CGCTCTGCGACACTACATCA; *Npy* Reverse: AGGGTCTTCAAGCCTTGTTCT; *Il13* Forward: CCAGACTCCCCTGTGCAAC; *Il13* Reverse: GGCTACACAGAACCCGCC; *Muc5ac* Forward: AAGATCAACTGTCCGCAGGG; *Muc5ac* Reverse: GGTGCACCGTACATTTCTGC; *Muc5b* Forward: AAGAGCACAGAGTGTCAGGC; *Muc5b* Reverse: GTGTGTGGCAGCTTTTGAGG.

**Western Blot.** C57BL6 mice DRG or JNC neurons ($5x10^3$; 200 µL) were plated onto 96 well plates and cultured overnight. Neurons were exposed to IL-13 or vehicle for 60 minutes (37°), then washed with PBS and lysed in RIPA buffer (Sigma, #20-188) supplemented with phosphatase inhibitor (1/100, Sigma #P0044) and protease inhibitor (1/200, Sigma, #P1860) for 20 minutes at room temperature. Protein concentrations were measured by BCA (Thermofisher, #23227) and equilibrated with a supplemented RIPA buffer. Samples were then mixed 1:1 with loading buffer (0.1M Tris pH 6.8; 4% SDS; 0.25% Bromophenol blue; 20% glycerol; 10% β-mercaptoethanol) and heated to denature proteins (100 °C, 5 minutes). 10 µg of protein were loaded and separated by SDS-PAGE electrophoresis with an acrylamide gel. Proteins were then transferred to a nitrocellulosis membrane, blocked with blocking buffer (TBS-T buffer containing 5% BSA), incubated with primary antibodies in blocking buffer (overnight, 4°), washed, and incubated with secondary antibodies in blocking buffer (1 h, RT). Membranes were then washed and revealed using SuperSignal West Dura Extended Duration Substrate (Thermofisher, #34075). Antibodies used included rabbit anti-pSTAT6 (1/1000, CST, #9361S), rabbit anti-STAT6 (1/1000, CST, #9362S) and HRP anti-rabbit (1/2000, CST, #7074S).

**Immunofluorescence.** C56BL6 and $Na_V1.8^{cre}$::$tdTomato^{fl/wt}$ mice were anesthetized with urethane (20%, 250 µL, i.p.) and perfused with 10 mL PBS, then with 10 mL 4% PFA. Lungs, JNC, DRG and SCG were harvested and

incubated in 4% PFA for 24 hours at 4°. Organs were then sequentially transferred in 10%, 20%, then 30% sucrose (24 hours each), before mounting and freezing (−80°) in OCT. Cryosections of 40 µm for lungs and 15 µm for ganglia were prepared. For neuron cultures, the medium was removed, and the cells fixed with 4% PFA for 15 minutes. Sections and cultures were incubated in blocking solution (1X PBS, 0.2% Triton X-100, 50 mg/mL BSA and 5% goat serum) for 3 hours at room temperature, then incubated with primary antibodies in staining solution (PBS, 0.2% Triton X-100 and 3% goat serum) for 48 hours at 4°. Primary antibodies used included rabbit anti-NPY (1/500, CST #11976S), guinea pig anti-PGP9.5 (1/1000, Sigma #AB5898), chicken anti-TH (1/500, Aves Laboratory #TYH-0020), rat anti-CD45 BV421 conjugated (1/300, Biolegend ##103134), rabbit anti-IL6 (1/300, CST #12912T). Cryosections were then washed (3 times, 15 minutes with shaking) with PBS containing 0.2% Triton X-100. Secondary antibodies were incubated in staining solution for 16 hours at 4°. Secondary antibodies included AF488 goat anti-guinea pig (1/1000, Thermofisher #A11073), AF546 goat anti-guinea pig (1/1000, Thermofisher #A-11074) AF647 goat anti-rabbit (1/1000, Thermofisher #A21245), CF488 goat anti-chicken (1/1000, Sigma #SAB4600039), AF405 goat anti-chicken (1/1000, Thermofisher #A48260). Ti2 microscope (Nikon) equipped with a camera (Photometrics Prime 95B 25 mm) was used for imaging. Nerve endings in lung slices were acquired by confocal microscopy (Zeiss, LSM800), with a Z stack of the whole section (40 µm).

**Immunofluorescence analysis.** Using ImageJ or Nikon Elements, circular ROI were defined based on PGP9.5 fluorescence for JNC and SG slices. For confocal pictures of lung slices, an orthogonal projection was made, then a threshold-based method was used to define the area of nerve fibers for each marker as well as their overlapping areas. Cultured cells were analyzed with a threshold-based method to define neurons based on tdTomato or PGP9.5 expression. All further analysis was performed in Microsoft Excel. When spillover between colors occurred, a compensation was applied using single-stain controls.

**Neuron culture for RNA sequencing.** $Na_V1.8^{cre}$::$tdTomato^{fl/wt}$ mice were sacrificed and their JNC harvested. For each sample, JNC from 2 males and 2 females were pooled and enzymatically dissociated, seeded ($1x10^4$ / well) in 12 well plate (VWR, #10062-894), and cultured with IL-13 (100 ng/mL) or its vehicle. After 24 hours, the cells were then mechanically detached with a cell scraper, sorted by flow cytometry, and collected into Trizol.

**RNA sequencing.** RNA libraries preparation and sequencing were carried out at the genomic platform of the Institut de Recherche en Cancérologie et en Immunologie (IRIC). Briefly, RNA quality was assessed using a Bioanalyzer (Agilent), and all preparations had an RIN>7.5. Libraries were prepared using the KAPA mRNA HyperPrep Kit (KapaBiosystems #KR1352). All barcoded samples were then sequenced with a Nextseq500 (Illumina) with 75-cycle single-end read.

Genome alignment and differential expression analysis were carried out (IRIC genomic platform). Sequences were trimmed for sequencing adapters and low quality 3' bases using Trimmomatic version 0.35 and aligned to the reference mouse genome version GRCm38 (gene annotation from Gencode version M25, based on Ensembl 100) using STAR version 2.7.1. Gene expressions were obtained from STAR as readcounts and computed using RSEM to obtain normalized gene and transcript level expression in FPKM. Differential expression analysis for the various comparisons of interest were made using DESeq (167) and STAR readcounts. Further analysis and plots were made using RStudio or Microsoft Excel. Genes were considered as differentially expressed if their adjusted p-value (FDR) was less than 0.2.

***In-silico* analysis of JNC neuron single-cell transcriptome:** Prescott et al.(1) generated single-cell sequencing data for nodose ganglia cells from 40 mice using the 10X Genomics platform. The data was downloaded from the NCBI Gene Expression Omnibus (GSE145216) and analyzed using Seurat. Neuronal cells were selected based on *Slc17a6* (VGLUT2) expression (raw count ≥ 2). A standard workflow was used for quality control, preprocessing, normalization, and clustering (resolution = 0.2, PCs = 1:30). *Phox2b* and *Prdm12* were used to identify nodose and jugular groups, while nociceptor neurons and low-threshold sensory neurons were defined based on their expression of *Scn10a* and *Scn1a (2)*.

**GSEA analysis:** Gene set enrichment analysis (168) was performed to compare similarities between different sequencing results together using the GSEA software. To assess the likelihood of scRNAseq neuron clusters innervating the airways, GSEA analysis was performed using the cluster markers identified by Seurat as genesets, and the DESeq2 counts of airway and visceral neurons as gene expression dataset. To compare nerve injury and

AAI signature, RNAseq data from Cobos et al (31) was downloaded from NCBI Gene Expression Omnibus (GSE102937) and reanalyzed by DESeq2. The top 100 overexpressed genes identified three days after nerve injury (Log2FC > 0,5, 100 lowest p-values) were used as a geneset (**supplementary table 3**), and DESeq2 counts of naive and AAI airway nociceptors as a gene expression dataset. Finally, the IL-13-induced geneset (adjusted p-value < 0.2) was compared to Deseq2 counts of naive and AAI airway neurons as a gene expression dataset.

**Data availability.** Bulk RNA-seq raw and processed data have been deposited in the NCBI's gene expression omnibus (GSE223355). Processed data can also be accessed using the browsing tool on our website (link pending) and in the **supplementary tables 1–5**. Additional information and raw data are available from the lead contact upon reasonable request.

**Statistics**. No data were excluded. P *values ≤ 0.05* were considered statistically significant**.** One-way ANOVA, two-way ANOVA, and Student t-tests were performed using Graphpad Prism. DESeq2 and Seurat analysis and statistics were performed using RStudio.

**Replicates**. Replicates ($n$) are described in the figure legends and represent the number of animals for *in vivo* data. For *in vitro* data, replicates can either be culture wells or dishes, animals, fields-of-view (microscopy), or neurons (patch-clamp), but always include preparations from different animals to ensure biological reproducibility.

**Acknowledgements.** This work was supported by the Canada Research Chair program (950-231859), the Canadian Institutes of Health Research (407016, 461274, 461275 to ST; 169160 to RB), the Canadian Foundation for Innovation (37439), and the Natural Sciences and Engineering Research Council of Canada (RGPIN-2019-06824 to ST, and RGPIN-2017-06871 to RB). SB received a fellowship from the centre interdisciplinaire de recherche sur le cerveau et apprentissage (CIRCA). We thank the genomic platform of the Institut de recherche en Cancérologie and Immunologie (IRIC), P. Gendron for the bioinformatic analysis, and R. Lambert and J. Huber for library preparation and sequencing. We also thank P.D.B. Rosa for graphic design.

**REFERENCES**


1. Prescott SL, Umans BD, Williams EK, Brust RD, and Liberles SD. An Airway Protection Program Revealed by Sweeping Genetic Control of Vagal Afferents. *Cell.* 2020;181(3):574-89 e14.
2. Kupari J, Haring M, Agirre E, Castelo-Branco G, and Ernfors P. An Atlas of Vagal Sensory Neurons and Their Molecular Specialization. *Cell Rep.* 2019;27(8):2508-23 e4.
3. Usoskin D, Furlan A, Islam S, Abdo H, Lonnerberg P, Lou D, et al. Unbiased classification of sensory neuron types by large-scale single-cell RNA sequencing. *Nat Neurosci.* 2015;18(1):145-53.
4. Dubin AE, and Patapoutian A. Nociceptors: the sensors of the pain pathway. *J Clin Invest.* 2010;120(11):3760-72.
5. Crosson T, Roversi K, Balood M, Othman R, Ahmadi M, Wang JC, et al. Profiling of how nociceptor neurons detect danger - new and old foes. *J Intern Med.* 2019;286(3):268-89.
6. Crosson T, and Talbot S. Anatomical differences in nociceptor neurons sensitivity. *Bioelectron Med.* 2022;8(1):7.
7. Zhao Q, Yu CD, Wang R, Xu QJ, Dai Pra R, Zhang L, et al. A multidimensional coding architecture of the vagal interoceptive system. *Nature.* 2022;603(7903):878-84.
8. Prescott SL, and Liberles SD. Internal senses of the vagus nerve. *Neuron.* 2022;110(4):579-99.
9. Canning BJ, Mori N, and Mazzone SB. Vagal afferent nerves regulating the cough reflex. *Respir Physiol Neurobiol.* 2006;152(3):223-42.
10. Oetjen LK, Mack MR, Feng J, Whelan TM, Niu H, Guo CJ, et al. Sensory Neurons Co-opt Classical Immune Signaling Pathways to Mediate Chronic Itch. *Cell.* 2017;171(1):217-28 e13.
11. Pinho-Ribeiro FA, Verri WA, Jr., and Chiu IM. Nociceptor Sensory Neuron-Immune Interactions in Pain and Inflammation. *Trends Immunol.* 2017;38(1):5-19.
12. Crosson T, Wang JC, Doyle B, Merrison H, Balood M, Parrin A, et al. FcepsilonR1-expressing nociceptors trigger allergic airway inflammation. *J Allergy Clin Immunol.* 2021;147(6):2330-42.
13. Chiu IM, von Hehn CA, and Woolf CJ. Neurogenic inflammation and the peripheral nervous system in host defense and immunopathology. *Nat Neurosci.* 2012;15(8):1063-7.
14. Talbot S, Abdulnour RE, Burkett PR, Lee S, Cronin SJ, Pascal MA, et al. Silencing Nociceptor Neurons Reduces Allergic Airway Inflammation. *Neuron.* 2015;87(2):341-54.
15. Serhan N, Basso L, Sibilano R, Petitfils C, Meixiong J, Bonnart C, et al. House dust mites activate nociceptor-mast cell clusters to drive type 2 skin inflammation. *Nat Immunol.* 2019;20(11):1435-43.
16. Perner C, Flayer CH, Zhu X, Aderhold PA, Dewan ZNA, Voisin T, et al. Substance P Release by Sensory Neurons Triggers Dendritic Cell Migration and Initiates the Type-2 Immune Response to Allergens. *Immunity.* 2020;53(5):1063-77 e7.
17. Cohen JA, Edwards TN, Liu AW, Hirai T, Jones MR, Wu J, et al. Cutaneous TRPV1(+) Neurons Trigger Protective Innate Type 17 Anticipatory Immunity. *Cell.* 2019;178(4):919-32 e14.
18. Chapman LF. Mechanisms of the flare reaction in human skin. *J Invest Dermatol.* 1977;69(1):88-97.
19. Szolcsanyi J. Antidromic vasodilatation and neurogenic inflammation. *Agents Actions.* 1988;23(1-2):4-11.
20. Tracey KJ. The inflammatory reflex. *Nature.* 2002;420(6917):853-9.
21. Talbot S, Doyle B, Huang J, Wang JC, Ahmadi M, Roberson DP, et al. Vagal sensory neurons drive mucous cell metaplasia. *J Allergy Clin Immunol.* 2020;145(6):1693-6 e4.
22. Trankner D, Hahne N, Sugino K, Hoon MA, and Zuker C. Population of sensory neurons essential for asthmatic hyperreactivity of inflamed airways. *Proc Natl Acad Sci U S A.* 2014;111(31):11515-20.
23. Balestrini A, Joseph V, Dourado M, Reese RM, Shields SD, Rouge L, et al. A TRPA1 inhibitor suppresses neurogenic inflammation and airway contraction for asthma treatment. *J Exp Med.* 2021;218(4).

24. Chavan SS, Pavlov VA, and Tracey KJ. Mechanisms and Therapeutic Relevance of Neuro-immune Communication. *Immunity.* 2017;46(6):927-42.
25. Chang RB, Strochlic DE, Williams EK, Umans BD, and Liberles SD. Vagal Sensory Neuron Subtypes that Differentially Control Breathing. *Cell.* 2015;161(3):622-33.
26. Sapio MR, Vazquez FA, Loydpierson AJ, Maric D, Kim JJ, LaPaglia DM, et al. Comparative Analysis of Dorsal Root, Nodose and Sympathetic Ganglia for the Development of New Analgesics. *Front Neurosci.* 2020;14:615362.
27. Caceres AI, Brackmann M, Elia MD, Bessac BF, del Camino D, D'Amours M, et al. A sensory neuronal ion channel essential for airway inflammation and hyperreactivity in asthma. *Proc Natl Acad Sci U S A.* 2009;106(22):9099-104.
28. Choi JY, Lee HY, Hur J, Kim KH, Kang JY, Rhee CK, et al. TRPV1 Blocking Alleviates Airway Inflammation and Remodeling in a Chronic Asthma Murine Model. *Allergy Asthma Immunol Res.* 2018;10(3):216-24.
29. Rehman R, Bhat YA, Panda L, and Mabalirajan U. TRPV1 inhibition attenuates IL-13 mediated asthma features in mice by reducing airway epithelial injury. *Int Immunopharmacol.* 2013;15(3):597-605.
30. Silverman HA, Tynan A, Hepler TD, Chang EH, Gunasekaran M, Li JH, et al. Transient Receptor Potential Ankyrin-1-expressing vagus nerve fibers mediate IL-1beta induced hypothermia and reflex anti-inflammatory responses. *Mol Med.* 2023;29(1):4.
31. Cobos EJ, Nickerson CA, Gao F, Chandran V, Bravo-Caparros I, Gonzalez-Cano R, et al. Mechanistic Differences in Neuropathic Pain Modalities Revealed by Correlating Behavior with Global Expression Profiling. *Cell Rep.* 2018;22(5):1301-12.
32. O'Shea JJ, Gadina M, and Schreiber RD. Cytokine signaling in 2002: new surprises in the Jak/Stat pathway. *Cell.* 2002;109 Suppl:S121-31.
33. Yan Y, Ramanan D, Rozenberg M, McGovern K, Rastelli D, Vijaykumar B, et al. Interleukin-6 produced by enteric neurons regulates the number and phenotype of microbe-responsive regulatory T cells in the gut. *Immunity.* 2021;54(3):499-513 e5.
34. Alhadeff AL, Su Z, Hernandez E, Klima ML, Phillips SZ, Holland RA, et al. A Neural Circuit for the Suppression of Pain by a Competing Need State. *Cell.* 2018;173(1):140-52 e15.
35. Gao T, Ma H, Xu B, Bergman J, Larhammar D, and Lagerstrom MC. The Neuropeptide Y System Regulates Both Mechanical and Histaminergic Itch. *J Invest Dermatol.* 2018;138(11):2405-11.
36. Nelson TS, Sinha GP, Santos DFS, Jukkola P, Prasoon P, Winter MK, et al. Spinal neuropeptide Y Y1 receptor-expressing neurons are a pharmacotherapeutic target for the alleviation of neuropathic pain. *Proc Natl Acad Sci U S A.* 2022;119(46):e2204515119.
37. Intondi AB, Dahlgren MN, Eilers MA, and Taylor BK. Intrathecal neuropeptide Y reduces behavioral and molecular markers of inflammatory or neuropathic pain. *Pain.* 2008;137(2):352-65.
38. Naveilhan P, Hassani H, Lucas G, Blakeman KH, Hao JX, Xu XJ, et al. Reduced antinociception and plasma extravasation in mice lacking a neuropeptide Y receptor. *Nature.* 2001;409(6819):513-7.
39. Acton D, Ren X, Di Costanzo S, Dalet A, Bourane S, Bertocchi I, et al. Spinal Neuropeptide Y1 Receptor-Expressing Neurons Form an Essential Excitatory Pathway for Mechanical Itch. *Cell Rep.* 2019;28(3):625-39 e6.
40. Chen L, Hu Y, Wang S, Cao K, Mai W, Sha W, et al. mTOR-neuropeptide Y signaling sensitizes nociceptors to drive neuropathic pain. *JCI Insight.* 2022;7(22).
41. Gibbs JL, Flores CM, and Hargreaves KM. Attenuation of capsaicin-evoked mechanical allodynia by peripheral neuropeptide Y Y1 receptors. *Pain.* 2006;124(1-2):167-74.
42. Tracey DJ, Romm MA, and Yao NN. Peripheral hyperalgesia in experimental neuropathy: exacerbation by neuropeptide Y. *Brain Res.* 1995;669(2):245-54.
43. Oda N, Miyahara N, Taniguchi A, Morichika D, Senoo S, Fujii U, et al. Requirement for neuropeptide Y in the development of type 2 responses and allergen-induced airway hyperresponsiveness and inflammation. *Am J Physiol Lung Cell Mol Physiol.* 2019;316(3):L407-L17.
44. Herzog H, Hort YJ, Ball HJ, Hayes G, Shine J, and Selbie LA. Cloned human neuropeptide Y receptor couples to two different second messenger systems. *Proc Natl Acad Sci U S A.* 1992;89(13):5794-8.

45. Roberson DP, Gudes S, Sprague JM, Patoski HA, Robson VK, Blasl F, et al. Activity-dependent silencing reveals functionally distinct itch-generating sensory neurons. *Nat Neurosci.* 2013;16(7):910-8.
46. Huang CC, Yang W, Guo C, Jiang H, Li F, Xiao M, et al. Anatomical and functional dichotomy of ocular itch and pain. *Nat Med.* 2018;24(8):1268-76.
47. Harford TJ, Rezaee F, Scheraga RG, Olman MA, and Piedimonte G. Asthma predisposition and respiratory syncytial virus infection modulate transient receptor potential vanilloid 1 function in children's airways. *J Allergy Clin Immunol.* 2018;141(1):414-6 e4.
48. Chen Y, Wu X, Yang X, Liu X, Zeng Y, and Li J. Melatonin antagonizes ozone-exacerbated asthma by inhibiting the TRPV1 channel and stabilizing the Nrf2 pathway. *Environ Sci Pollut Res Int.* 2021;28(42):59858-67.
49. Mazzone SB, and Undem BJ. Vagal Afferent Innervation of the Airways in Health and Disease. *Physiol Rev.* 2016;96(3):975-1024.
50. Kaelberer MM, Caceres AI, and Jordt SE. Activation of a nerve injury transcriptional signature in airway-innervating sensory neurons after lipopolysaccharide-induced lung inflammation. *Am J Physiol Lung Cell Mol Physiol.* 2020;318(5):L953-L64.
51. Zhang H, Li Y, de Carvalho-Barbosa M, Kavelaars A, Heijnen CJ, Albrecht PJ, et al. Dorsal Root Ganglion Infiltration by Macrophages Contributes to Paclitaxel Chemotherapy-Induced Peripheral Neuropathy. *J Pain.* 2016;17(7):775-86.
52. Yu X, Liu H, Hamel KA, Morvan MG, Yu S, Leff J, et al. Dorsal root ganglion macrophages contribute to both the initiation and persistence of neuropathic pain. *Nat Commun.* 2020;11(1):264.
53. Calvo M, and Bennett DL. The mechanisms of microgliosis and pain following peripheral nerve injury. *Exp Neurol.* 2012;234(2):271-82.
54. Hu P, Bembrick AL, Keay KA, and McLachlan EM. Immune cell involvement in dorsal root ganglia and spinal cord after chronic constriction or transection of the rat sciatic nerve. *Brain Behav Immun.* 2007;21(5):599-616.
55. Raoof R, Martin Gil C, Lafeber F, de Visser H, Prado J, Versteeg S, et al. Dorsal Root Ganglia Macrophages Maintain Osteoarthritis Pain. *J Neurosci.* 2021;41(39):8249-61.
56. Foster SL, Seehus CR, Woolf CJ, and Talbot S. Sense and Immunity: Context-Dependent Neuro-Immune Interplay. *Front Immunol.* 2017;8:1463.
57. Hu Z, Deng N, Liu K, Zhou N, Sun Y, and Zeng W. CNTF-STAT3-IL-6 Axis Mediates Neuroinflammatory Cascade across Schwann Cell-Neuron-Microglia. *Cell Rep.* 2020;31(7):107657.
58. Ben-Yaakov K, Dagan SY, Segal-Ruder Y, Shalem O, Vuppalanchi D, Willis DE, et al. Axonal transcription factors signal retrogradely in lesioned peripheral nerve. *EMBO J.* 2012;31(6):1350-63.
59. Shin JE, Cho Y, Beirowski B, Milbrandt J, Cavalli V, and DiAntonio A. Dual leucine zipper kinase is required for retrograde injury signaling and axonal regeneration. *Neuron.* 2012;74(6):1015-22.
60. Qiu J, Cafferty WB, McMahon SB, and Thompson SW. Conditioning injury-induced spinal axon regeneration requires signal transducer and activator of transcription 3 activation. *J Neurosci.* 2005;25(7):1645-53.
61. Melemedjian OK, Tillu DV, Moy JK, Asiedu MN, Mandell EK, Ghosh S, et al. Local translation and retrograde axonal transport of CREB regulates IL-6-induced nociceptive plasticity. *Mol Pain.* 2014;10:45.
62. Cox LJ, Hengst U, Gurskaya NG, Lukyanov KA, and Jaffrey SR. Intra-axonal translation and retrograde trafficking of CREB promotes neuronal survival. *Nat Cell Biol.* 2008;10(2):149-59.
63. Masato Tamari KLDB, Aaron M. Ver Heul,8 Lydia Zamidar, Keisuke Orimo, Masato Hoshi, Anna M. Trier, Ting-Lin Yang, Catherine M. Biggs, Gargi Damle, Deniz Demircioglu, Dan Hasson, Jinye Dai, Hideaki Morita, Kenji Matsumoto, Sanjay Jain, Steven Van Dyken, Joshua D. Milner,19 Dusan Bogunovic, Hongzhen Hu, David Artis, Stuart E. Turvey, Brian S. Kim. Sensory Neurons Promote Immune Homeostasis in the Lung. *Under review.* 2022.
64. Katie H. Barker JPH, Luke A. Pattison, Iain P. Chessell, Fraser Welsh, View ORCID ProfileEwan St. J. Smith, David C. Bulmer. Sensitisation of colonic nociceptors by IL-13 is dependent on JAK and p38 MAPK activity. *Biorxiv.* 2022.
65. Walford HH, and Doherty TA. STAT6 and lung inflammation. *JAKSTAT.* 2013;2(4):e25301.

66. Bao L, Zhang H, and Chan LS. The involvement of the JAK-STAT signaling pathway in chronic inflammatory skin disease atopic dermatitis. *JAKSTAT.* 2013;2(3):e24137.
67. Kim BS. The translational revolution of itch. *Neuron.* 2022;110(14):2209-14.
68. Rincon M, and Irvin CG. Role of IL-6 in asthma and other inflammatory pulmonary diseases. *Int J Biol Sci.* 2012;8(9):1281-90.
69. Yokoyama A, Kohno N, Fujino S, Hamada H, Inoue Y, Fujioka S, et al. Circulating interleukin-6 levels in patients with bronchial asthma. *Am J Respir Crit Care Med.* 1995;151(5):1354-8.
70. Neveu WA, Allard JB, Dienz O, Wargo MJ, Ciliberto G, Whittaker LA, et al. IL-6 is required for airway mucus production induced by inhaled fungal allergens. *J Immunol.* 2009;183(3):1732-8.
71. Diehl S, Chow CW, Weiss L, Palmetshofer A, Twardzik T, Rounds L, et al. Induction of NFATc2 expression by interleukin 6 promotes T helper type 2 differentiation. *J Exp Med.* 2002;196(1):39-49.
72. Yang Y, Ochando J, Yopp A, Bromberg JS, and Ding Y. IL-6 plays a unique role in initiating c-Maf expression during early stage of CD4 T cell activation. *J Immunol.* 2005;174(5):2720-9.
73. Diehl S, Anguita J, Hoffmeyer A, Zapton T, Ihle JN, Fikrig E, et al. Inhibition of Th1 differentiation by IL-6 is mediated by SOCS1. *Immunity.* 2000;13(6):805-15.
74. Bettelli E, Carrier Y, Gao W, Korn T, Strom TB, Oukka M, et al. Reciprocal developmental pathways for the generation of pathogenic effector TH17 and regulatory T cells. *Nature.* 2006;441(7090):235-8.
75. Dominitzki S, Fantini MC, Neufert C, Nikolaev A, Galle PR, Scheller J, et al. Cutting edge: trans-signaling via the soluble IL-6R abrogates the induction of FoxP3 in naive CD4+CD25 T cells. *J Immunol.* 2007;179(4):2041-5.
76. Qiu Z, Fujimura M, Kurashima K, Nakao S, and Mukaida N. Enhanced airway inflammation and decreased subepithelial fibrosis in interleukin 6-deficient mice following chronic exposure to aerosolized antigen. *Clin Exp Allergy.* 2004;34(8):1321-8.
77. Blesch A, Lu P, Tsukada S, Alto LT, Roet K, Coppola G, et al. Conditioning lesions before or after spinal cord injury recruit broad genetic mechanisms that sustain axonal regeneration: superiority to camp-mediated effects. *Exp Neurol.* 2012;235(1):162-73.
78. Greenberg S, Chang P, and Silverstein SC. Tyrosine phosphorylation is required for Fc receptor-mediated phagocytosis in mouse macrophages. *J Exp Med.* 1993;177(2):529-34.
79. Ferreira SH, Lorenzetti BB, and De Campos DI. Induction, blockade and restoration of a persistent hypersensitive state. *Pain.* 1990;42(3):365-71.
80. Taiwo YO, Bjerknes LK, Goetzl EJ, and Levine JD. Mediation of primary afferent peripheral hyperalgesia by the cAMP second messenger system. *Neuroscience.* 1989;32(3):577-80.
81. Taiwo YO, and Levine JD. Further confirmation of the role of adenyl cyclase and of cAMP-dependent protein kinase in primary afferent hyperalgesia. *Neuroscience.* 1991;44(1):131-5.
82. Kress M, Rodl J, and Reeh PW. Stable analogues of cyclic AMP but not cyclic GMP sensitize unmyelinated primary afferents in rat skin to heat stimulation but not to inflammatory mediators, in vitro. *Neuroscience.* 1996;74(2):609-17.
83. England S, Bevan S, and Docherty RJ. PGE2 modulates the tetrodotoxin-resistant sodium current in neonatal rat dorsal root ganglion neurones via the cyclic AMP-protein kinase A cascade. *J Physiol.* 1996;495 ( Pt 2)(Pt 2):429-40.
84. Fitzgerald EM, Okuse K, Wood JN, Dolphin AC, and Moss SJ. cAMP-dependent phosphorylation of the tetrodotoxin-resistant voltage-dependent sodium channel SNS. *J Physiol.* 1999;516 ( Pt 2)(Pt 2):433-46.
85. Mercer RE, Chee MJ, and Colmers WF. The role of NPY in hypothalamic mediated food intake. *Front Neuroendocrinol.* 2011;32(4):398-415.
86. Zhang W, Cline MA, and Gilbert ER. Hypothalamus-adipose tissue crosstalk: neuropeptide Y and the regulation of energy metabolism. *Nutr Metab (Lond).* 2014;11:27.
87. Han S, Yang CL, Chen X, Naes L, Cox BF, and Westfall T. Direct evidence for the role of neuropeptide Y in sympathetic nerve stimulation-induced vasoconstriction. *Am J Physiol.* 1998;274(1):H290-4.
88. Wheway J, Herzog H, and Mackay F. NPY and receptors in immune and inflammatory diseases. *Curr Top Med Chem.* 2007;7(17):1743-52.

89. Li S, Koziol-White C, Jude J, Jiang M, Zhao H, Cao G, et al. Epithelium-generated neuropeptide Y induces smooth muscle contraction to promote airway hyperresponsiveness. *J Clin Invest.* 2016;126(5):1978-82.
90. Makinde TO, Steininger R, and Agrawal DK. NPY and NPY receptors in airway structural and inflammatory cells in allergic asthma. *Exp Mol Pathol.* 2013;94(1):45-50.
91. Sui P, Wiesner DL, Xu J, Zhang Y, Lee J, Van Dyken S, et al. Pulmonary neuroendocrine cells amplify allergic asthma responses. *Science.* 2018;360(6393).
92. Macia L, Rao PT, Wheway J, Sierro F, Mackay F, and Herzog H. Y1 signalling has a critical role in allergic airway inflammation. *Immunol Cell Biol.* 2011;89(8):882-8.
93. Dahlof C, Dahlof P, Lundberg JM, and Strombom U. Elevated plasma concentration of neuropeptide Y and low level of circulating adrenaline in elderly asthmatics during rest and acute severe asthma. *Pulm Pharmacol.* 1988;1(1):3-6.
94. Zhou YQ, Liu Z, Liu ZH, Chen SP, Li M, Shahveranov A, et al. Interleukin-6: an emerging regulator of pathological pain. *J Neuroinflammation.* 2016;13(1):141.
95. Story GM, Peier AM, Reeve AJ, Eid SR, Mosbacher J, Hricik TR, et al. ANKTM1, a TRP-like channel expressed in nociceptive neurons, is activated by cold temperatures. *Cell.* 2003;112(6):819-29.
96. Defaye M, Iftinca MC, Gadotti VM, Basso L, Abdullah NS, Cumenal M, et al. The neuronal tyrosine kinase receptor ligand ALKAL2 mediates persistent pain. *J Clin Invest.* 2022;132(12).
97. Sikandar S, Minett MS, Millet Q, Santana-Varela S, Lau J, Wood JN, et al. Brain-derived neurotrophic factor derived from sensory neurons plays a critical role in chronic pain. *Brain.* 2018;141(4):1028-39.
98. Fairbanks CA, Peterson CD, Speltz RH, Riedl MS, Kitto KF, Dykstra JA, et al. The VGF-derived peptide TLQP-21 contributes to inflammatory and nerve injury-induced hypersensitivity. *Pain.* 2014;155(7):1229-37.
99. Yu X, Ton AN, Niu Z, Morales BM, Chen J, Braz J, et al. ACVR1-activating mutation causes neuropathic pain and sensory neuron hyperexcitability in humans. *Pain.* 2023;164(1):43-58.
100. Mabuchi T, Shintani N, Matsumura S, Okuda-Ashitaka E, Hashimoto H, Muratani T, et al. Pituitary adenylate cyclase-activating polypeptide is required for the development of spinal sensitization and induction of neuropathic pain. *J Neurosci.* 2004;24(33):7283-91.
101. Yamada M, Fujita Y, Hayano Y, Hayakawa H, Baba K, Mochizuki H, et al. Increased Expression of Fibronectin Leucine-Rich Transmembrane Protein 3 in the Dorsal Root Ganglion Induces Neuropathic Pain in Rats. *J Neurosci.* 2019;39(38):7615-27.
102. Weng HJ, Patel KN, Jeske NA, Bierbower SM, Zou W, Tiwari V, et al. Tmem100 Is a Regulator of TRPA1-TRPV1 Complex and Contributes to Persistent Pain. *Neuron.* 2015;85(4):833-46.
103. Zhao JY, Yang L, Bai HH, Liu JP, Suo ZW, Yang X, et al. Inhibition of protein tyrosine phosphatase 1B in spinal cord dorsal horn of rats attenuated diabetic neuropathic pain. *Eur J Pharmacol.* 2018;827:189-97.
104. Kanehisa K, Koga K, Maejima S, Shiraishi Y, Asai K, Shiratori-Hayashi M, et al. Neuronal pentraxin 2 is required for facilitating excitatory synaptic inputs onto spinal neurons involved in pruriceptive transmission in a model of chronic itch. *Nat Commun.* 2022;13(1):2367.
105. Fang J, Yuan X, An X, Qu H, Wang C, Hong G, et al. Involvement of the Tetraspanin 2 (TSPAN2) Gene in Migraine: A Case-Control Study in Han Chinese. *Front Neurol.* 2018;9:714.
106. Santha P, Dobos I, Kis G, and Jancso G. Role of Gangliosides in Peripheral Pain Mechanisms. *Int J Mol Sci.* 2020;21(3).
107. Gross T, Wack G, Syhr KMJ, Tolmachova T, Seabra MC, Geisslinger G, et al. Rab27a Contributes to the Processing of Inflammatory Pain in Mice. *Cells.* 2020;9(6).
108. Jin M, Ishida M, Katoh-Fukui Y, Tsuchiya R, Higashinakagawa T, Ikegami S, et al. Reduced pain sensitivity in mice lacking latexin, an inhibitor of metallocarboxypeptidases. *Brain Res.* 2006;1075(1):117-21.
109. Zhang FF, Wang H, Zhou YM, Yu HY, Zhang M, Du X, et al. Inhibition of phosphodiesterase-4 in the spinal dorsal horn ameliorates neuropathic pain via cAMP-cytokine-Cx43 signaling in mice. *CNS Neurosci Ther.* 2022;28(5):749-60.

110. Crown ED, Gwak YS, Ye Z, Yu Tan H, Johnson KM, Xu GY, et al. Calcium/calmodulin dependent kinase II contributes to persistent central neuropathic pain following spinal cord injury. *Pain.* 2012;153(3):710-21.
111. Donnelly CR, Jiang C, Andriessen AS, Wang K, Wang Z, Ding H, et al. STING controls nociception via type I interferon signalling in sensory neurons. *Nature.* 2021;591(7849):275-80.
112. Vicuna L, Strochlic DE, Latremoliere A, Bali KK, Simonetti M, Husainie D, et al. The serine protease inhibitor SerpinA3N attenuates neuropathic pain by inhibiting T cell-derived leukocyte elastase. *Nat Med.* 2015;21(5):518-23.
113. Wheeler MA, Heffner DL, Kim S, Espy SM, Spano AJ, Cleland CL, et al. TNF-alpha/TNFR1 signaling is required for the development and function of primary nociceptors. *Neuron.* 2014;82(3):587-602.
114. Dominguez E, Mauborgne A, Mallet J, Desclaux M, and Pohl M. SOCS3-mediated blockade of JAK/STAT3 signaling pathway reveals its major contribution to spinal cord neuroinflammation and mechanical allodynia after peripheral nerve injury. *J Neurosci.* 2010;30(16):5754-66.
115. Emrick JJ, Mathur A, Wei J, Gracheva EO, Gronert K, Rosenblum MD, et al. Tissue-specific contributions of Tmem79 to atopic dermatitis and mast cell-mediated histaminergic itch. *Proc Natl Acad Sci U S A.* 2018;115(51):E12091-E100.
116. McGregor CE, and English AW. The Role of BDNF in Peripheral Nerve Regeneration: Activity-Dependent Treatments and Val66Met. *Front Cell Neurosci.* 2018;12:522.
117. Jing X, Wang T, Huang S, Glorioso JC, and Albers KM. The transcription factor Sox11 promotes nerve regeneration through activation of the regeneration-associated gene Sprr1a. *Exp Neurol.* 2012;233(1):221-32.
118. Nadjar Y, Triller A, Bessereau JL, and Dumoulin A. The Susd2 protein regulates neurite growth and excitatory synaptic density in hippocampal cultures. *Mol Cell Neurosci.* 2015;65:82-91.
119. Takahashi E, Sagane K, Nagasu T, and Kuromitsu J. Altered nociceptive response in ADAM11-deficient mice. *Brain Res.* 2006;1097(1):39-42.
120. Han SK, Mancino V, and Simon MI. Phospholipase Cbeta 3 mediates the scratching response activated by the histamine H1 receptor on C-fiber nociceptive neurons. *Neuron.* 2006;52(4):691-703.
121. Guo Z, Qiu CS, Jiang X, Zhang J, Li F, Liu Q, et al. TRESK K(+) Channel Activity Regulates Trigeminal Nociception and Headache. *eNeuro.* 2019;6(4).
122. Martinelli-Boneschi F, Colombi M, Castori M, Devigili G, Eleopra R, Malik RA, et al. COL6A5 variants in familial neuropathic chronic itch. *Brain.* 2017;140(3):555-67.
123. Liang Y, Xing X, Beamer MA, Swindell WR, Sarkar MK, Roberts LW, et al. Six-transmembrane epithelial antigens of the prostate comprise a novel inflammatory nexus in patients with pustular skin disorders. *J Allergy Clin Immunol.* 2017;139(4):1217-27.
124. Tanaka T, Narazaki M, and Kishimoto T. IL-6 in inflammation, immunity, and disease. *Cold Spring Harb Perspect Biol.* 2014;6(10):a016295.
125. Xie Y, Jiang H, Nguyen H, Jia S, Berro A, Panettieri RA, Jr., et al. Regulator of G protein signaling 2 is a key modulator of airway hyperresponsiveness. *J Allergy Clin Immunol.* 2012;130(4):968-76 e3.
126. Syme TE, Grill M, Hayashida E, Viengkhou B, Campbell IL, and Hofer MJ. Strawberry notch homolog 2 regulates the response to interleukin-6 in the central nervous system. *J Neuroinflammation.* 2022;19(1):126.
127. Snyder JM, Zhong G, Hogarth C, Huang W, Topping T, LaFrance J, et al. Knockout of Cyp26a1 and Cyp26b1 during postnatal life causes reduced lifespan, dermatitis, splenomegaly, and systemic inflammation in mice. *FASEB J.* 2020;34(12):15788-804.
128. Picotto G, Morse LR, Nguyen N, Saltzman J, and Battaglino R. TMEM176A and TMEM176B Are Candidate Regulators of Inhibition of Dendritic Cell Maturation and Function after Chronic Spinal Cord Injury. *J Neurotrauma.* 2020;37(3):528-33.
129. Kim HR, Lee HS, Lee KS, Jung ID, Kwon MS, Kim CH, et al. An Essential Role for TAGLN2 in Phagocytosis of Lipopolysaccharide-activated Macrophages. *Sci Rep.* 2017;7(1):8731.

130. Zhao MM, Yang WL, Yang FY, Zhang L, Huang WJ, Hou W, et al. Cathepsin L plays a key role in SARS-CoV-2 infection in humans and humanized mice and is a promising target for new drug development. *Signal Transduct Target Ther.* 2021;6(1):134.
131. Dreymueller D, Pruessmeyer J, Schumacher J, Fellendorf S, Hess FM, Seifert A, et al. The metalloproteinase ADAM8 promotes leukocyte recruitment in vitro and in acute lung inflammation. *Am J Physiol Lung Cell Mol Physiol.* 2017;313(3):L602-L14.
132. Liu H, Zeng L, Yang Y, Guo C, and Wang H. Bcl-3: A Double-Edged Sword in Immune Cells and Inflammation. *Front Immunol.* 2022;13:847699.
133. Huang C, Hatzi K, and Melnick A. Lineage-specific functions of Bcl-6 in immunity and inflammation are mediated by distinct biochemical mechanisms. *Nat Immunol.* 2013;14(4):380-8.
134. Gallman AE, Wolfreys FD, Nguyen DN, Sandy M, Xu Y, An J, et al. Abcc1 and Ggt5 support lymphocyte guidance through export and catabolism of S-geranylgeranyl-l-glutathione. *Sci Immunol.* 2021;6(60).
135. Carow B, and Rottenberg ME. SOCS3, a Major Regulator of Infection and Inflammation. *Front Immunol.* 2014;5:58.
136. Zaiss DMW, Gause WC, Osborne LC, and Artis D. Emerging functions of amphiregulin in orchestrating immunity, inflammation, and tissue repair. *Immunity.* 2015;42(2):216-26.
137. Yu X, Teng XL, Wang F, Zheng Y, Qu G, Zhou Y, et al. Metabolic control of regulatory T cell stability and function by TRAF3IP3 at the lysosome. *J Exp Med.* 2018;215(9):2463-76.
138. Markiewski MM, and Lambris JD. The role of complement in inflammatory diseases from behind the scenes into the spotlight. *Am J Pathol.* 2007;171(3):715-27.
139. Shen W, Chang A, Wang J, Zhou W, Gao R, Li J, et al. TIFA, an inflammatory signaling adaptor, is tumor suppressive for liver cancer. *Oncogenesis.* 2015;4(10):e173.
140. Sahu N, and August A. ITK inhibitors in inflammation and immune-mediated disorders. *Curr Top Med Chem.* 2009;9(8):690-703.
141. Lucas TM, Richner JM, and Diamond MS. The Interferon-Stimulated Gene Ifi27l2a Restricts West Nile Virus Infection and Pathogenesis in a Cell-Type- and Region-Specific Manner. *J Virol.* 2015;90(5):2600-15.
142. Prashar A, Schnettger L, Bernard EM, and Gutierrez MG. Rab GTPases in Immunity and Inflammation. *Front Cell Infect Microbiol.* 2017;7:435.
143. Adorno-Cruz V, and Liu H. Regulation and functions of integrin alpha2 in cell adhesion and disease. *Genes Dis.* 2019;6(1):16-24.
144. Hill RZ, Morita T, Brem RB, and Bautista DM. S1PR3 Mediates Itch and Pain via Distinct TRP Channel-Dependent Pathways. *J Neurosci.* 2018;38(36):7833-43.
145. Sun YG, and Chen ZF. A gastrin-releasing peptide receptor mediates the itch sensation in the spinal cord. *Nature.* 2007;448(7154):700-3.
146. Zhuang GZ, Keeler B, Grant J, Bianchi L, Fu ES, Zhang YP, et al. Carbonic anhydrase-8 regulates inflammatory pain by inhibiting the ITPR1-cytosolic free calcium pathway. *PLoS One.* 2015;10(3):e0118273.
147. Avrampou K, Pryce KD, Ramakrishnan A, Sakloth F, Gaspari S, Serafini RA, et al. RGS4 Maintains Chronic Pain Symptoms in Rodent Models. *J Neurosci.* 2019;39(42):8291-304.
148. Barragan-Iglesias P, Lou TF, Bhat VD, Megat S, Burton MD, Price TJ, et al. Inhibition of Poly(A)-binding protein with a synthetic RNA mimic reduces pain sensitization in mice. *Nat Commun.* 2018;9(1):10.
149. Tan PH, Ji J, Yeh CC, and Ji RR. Interferons in Pain and Infections: Emerging Roles in Neuro-Immune and Neuro-Glial Interactions. *Front Immunol.* 2021;12:783725.
150. Mohamad O, Song M, Wei L, and Yu SP. Regulatory roles of the NMDA receptor GluN3A subunit in locomotion, pain perception and cognitive functions in adult mice. *J Physiol.* 2013;591(1):149-68.
151. Gu JJ, Rouse C, Xu X, Wang J, Onaitis MW, and Pendergast AM. Inactivation of ABL kinases suppresses non-small cell lung cancer metastasis. *JCI Insight.* 2016;1(21):e89647.
152. Samuchiwal SK, and Balestrieri B. Harmful and protective roles of group V phospholipase A(2): Current perspectives and future directions. *Biochim Biophys Acta Mol Cell Biol Lipids.* 2019;1864(6):819-26.

153. Lawrence DW, Willard PA, Cochran AM, Matchett EC, and Kornbluth J. Natural Killer Lytic-Associated Molecule (NKLAM): An E3 Ubiquitin Ligase With an Integral Role in Innate Immunity. *Front Physiol.* 2020;11:573372.
154. John SP, Sun J, Carlson RJ, Cao B, Bradfield CJ, Song J, et al. IFIT1 Exerts Opposing Regulatory Effects on the Inflammatory and Interferon Gene Programs in LPS-Activated Human Macrophages. *Cell Rep.* 2018;25(1):95-106 e6.
155. Yurchenko M, Skjesol A, Ryan L, Richard GM, Kandasamy RK, Wang N, et al. SLAMF1 is required for TLR4-mediated TRAM-TRIF-dependent signaling in human macrophages. *J Cell Biol.* 2018;217(4):1411-29.
156. Meyer NJ, Huang Y, Singleton PA, Sammani S, Moitra J, Evenoski CL, et al. GADD45a is a novel candidate gene in inflammatory lung injury via influences on Akt signaling. *FASEB J.* 2009;23(5):1325-37.
157. Choubey D, Duan X, Dickerson E, Ponomareva L, Panchanathan R, Shen H, et al. Interferon-inducible p200-family proteins as novel sensors of cytoplasmic DNA: role in inflammation and autoimmunity. *J Interferon Cytokine Res.* 2010;30(6):371-80.
158. Takeshima H, Horie M, Mikami Y, Makita K, Miyashita N, Matsuzaki H, et al. CISH is a negative regulator of IL-13-induced CCL26 production in lung fibroblasts. *Allergol Int.* 2019;68(1):101-9.
159. Jones EL, Laidlaw SM, and Dustin LB. TRIM21/Ro52 - Roles in Innate Immunity and Autoimmune Disease. *Front Immunol.* 2021;12:738473.
160. Rozzo SJ, Allard JD, Choubey D, Vyse TJ, Izui S, Peltz G, et al. Evidence for an interferon-inducible gene, Ifi202, in the susceptibility to systemic lupus. *Immunity.* 2001;15(3):435-43.
161. Greter M, Helft J, Chow A, Hashimoto D, Mortha A, Agudo-Cantero J, et al. GM-CSF controls nonlymphoid tissue dendritic cell homeostasis but is dispensable for the differentiation of inflammatory dendritic cells. *Immunity.* 2012;36(6):1031-46.
162. Del Rosso M, Margheri F, Serrati S, Chilla A, Laurenzana A, and Fibbi G. The urokinase receptor system, a key regulator at the intersection between inflammation, immunity, and coagulation. *Curr Pharm Des.* 2011;17(19):1924-43.
163. Croft M, Duan W, Choi H, Eun SY, Madireddi S, and Mehta A. TNF superfamily in inflammatory disease: translating basic insights. *Trends Immunol.* 2012;33(3):144-52.
164. Takano M, Hirose N, Sumi C, Yanoshita M, Nishiyama S, Onishi A, et al. ANGPTL2 Promotes Inflammation via Integrin alpha5beta1 in Chondrocytes. *Cartilage.* 2021;13(2_suppl):885S-97S.
165. Parker D. CD80/CD86 signaling contributes to the proinflammatory response of Staphylococcus aureus in the airway. *Cytokine.* 2018;107:130-6.
166. Sheng L, Luo Q, and Chen L. Amino Acid Solute Carrier Transporters in Inflammation and Autoimmunity. *Drug Metab Dispos.* 2022.
167. Love MI, Huber W, and Anders S. Moderated estimation of fold change and dispersion for RNA-seq data with DESeq2. *Genome Biol.* 2014;15(12):550.
168. Subramanian A, Tamayo P, Mootha VK, Mukherjee S, Ebert BL, Gillette MA, et al. Gene set enrichment analysis: a knowledge-based approach for interpreting genome-wide expression profiles. *Proc Natl Acad Sci U S A.* 2005;102(43):15545-50.